



Review of experimental techniques for high rate deformation and shock studies

J.E. Field, S.M. Walley*, W.G. Proud, H.T. Goldrein, C.R. Siviour

Cavendish Laboratory, Physics and Chemistry of Solids (PCS), Madingley Road, Cambridge CB3 0HE, UK

Accepted 16 March 2004

Abstract

A variety of techniques used to obtain the mechanical properties of materials at high rates of strain ($\geq 10 \text{ s}^{-1}$) are summarised. These include dropweight machines, split Hopkinson pressure bars, Taylor impact and shock loading by plate impact. High-speed photography, particularly when used in association with optical techniques, is a key area and recent advances and applications to studies of ballistic impact are discussed. More comprehensive bibliographies and a fuller discussion of the history may be found in earlier reviews published by us in 1994, 1998 and 2001 (J Phys IV France 4 (C8) (1994) 3; Review of experimental techniques for high rate deformation studies, Proceedings of the Acoustics and Vibration Asia '98, Acoustics and Vibration Asia 98 Conference, Singapore, 1998; Review of experimental techniques for high rate deformation and shock studies, New Experimental Methods in Material Dynamics and Impact, Institute of Fundamental Technological Research, Warsaw, Poland, 2001).

© 2004 Elsevier Ltd. All rights reserved.

Keywords: Hopkinson bar; Taylor impact; Plate impact; Dropweight; Ballistic impact; Shockloading; High speed photography; Optical techniques; Moiré; Speckle; Fragmentation

1. Introduction

This paper updates previous review articles published by us on the topic of high rate studies of materials [1–3]. A fuller discussion of the history of the subject may be found there. Fig. 1 presents a schematic diagram of the range of strain rates (in reciprocal seconds) that are typically of interest to materials scientists. They span 16 orders of magnitude from creep (over periods of

*Corresponding author. Tel.: +44-1223-339375; fax: +44-1223-350-266.

E-mail address: smw14@phy.cam.ac.uk (S.M. Walley).

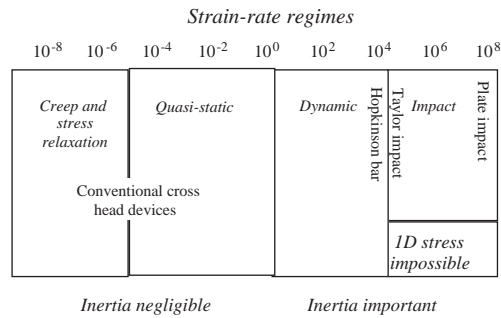


Fig. 1. Schematic diagram of strain rate regimes (in reciprocal seconds) and the techniques that have been developed for obtaining them.

years) to shock (nanoseconds). Conventional commercial mechanical testing machines cover the low strain rate range up to around 10 s^{-1} . Dropweight machines are also available commercially and standards have been written covering their design and use in the strain rate range $10\text{--}1000\text{ s}^{-1}$. Historically, machines for obtaining mechanical data at higher rates of deformation have tended to be confined to government or university laboratories, but recently some companies have been ‘spun-off’ to market items such as split Hopkinson pressure bars (SHPBs) and plate impact facilities.

One very important transition that this figure shows is that from a state of one-dimensional (1D) stress to 1D strain. The strain rate at which this occurs depends on the density of the material being investigated and the size of the specimen: the larger the specimen and the higher its density, the lower the transitional strain rate [4,5]. Examples of the effect of strain rate on mechanical properties combined with the transition from 1D stress to 1D strain are given in Fig. 2. The transition is due to inertial confinement of the material as may be seen from the graph presented in Fig. 3.

Because it is necessary to have about 1000 grains or crystals in a specimen for it to be mechanically representative of the bulk [8,9], the coarser the microstructure, the larger the specimen has to be to fulfil this condition and hence the lower the maximum strain rate that can be accessed in 1D stress. Hence for investigating concrete, for example, very large Hopkinson bars have had to be constructed [10]. By contrast, very fine-grained metals can be deformed in 1D stress at strain rates close to 10^5 s^{-1} using miniaturised Hopkinson bars (3 mm diameter) and 1 mm sized specimens [5,11].

Fuller historical surveys of the development of high strain rate techniques may be found in Refs. [3,12]. Recent reviews of the techniques outlined in this paper may be found in Ref. [13]. In addition, the DYMAT Association is in the process of publishing test recommendations. Those for compression Hopkinson bars [14] and Taylor impact [15] are already available; that for shock loading by plate impact will be published soon (see the website www.dymat.org).

2. Dropweights

Machines where a falling weight is used to strike a plaque or a structure are widely used in industry both in research and in quality control. The weight is often used to carry darts of various shapes (sharp, rounded) to impact the target. ASTM Standards have been written governing the

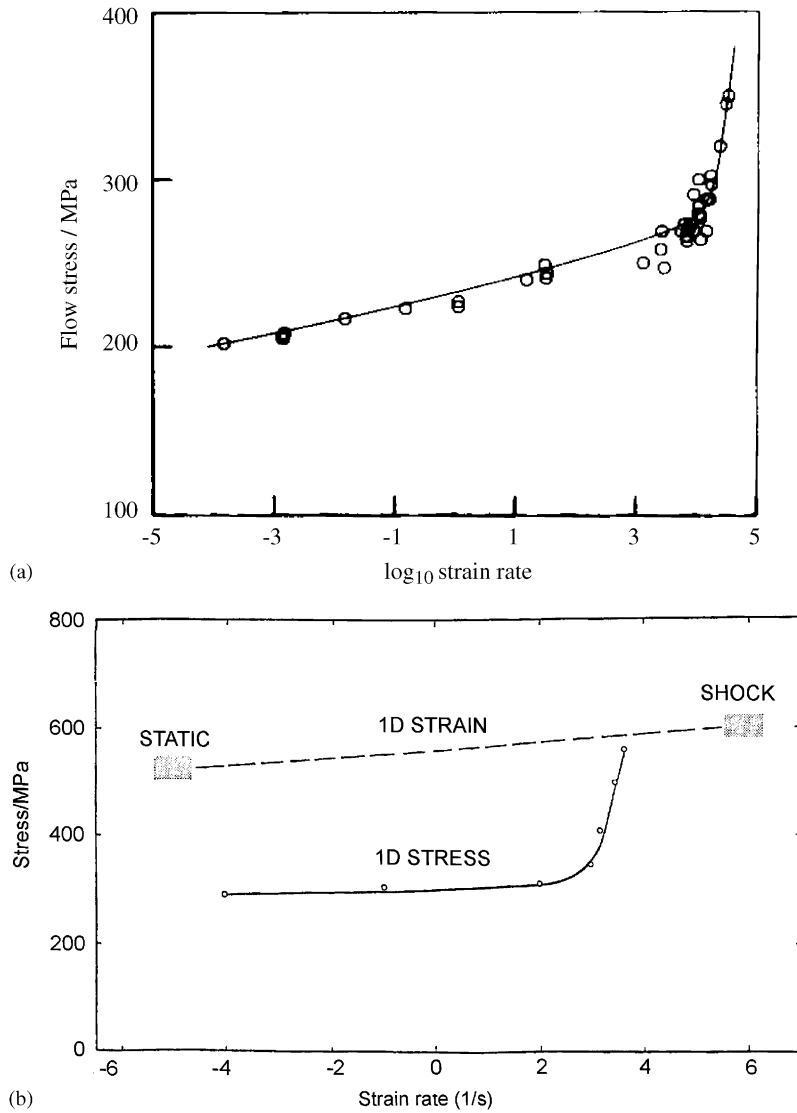


Fig. 2. (a) Plot of flow stress of copper as a function of $\log_{10}(\text{strain rate})$. From Ref. [6]. (b) Failure stress of limestone as a function both of strain rate and loading state. From Ref. [7].

performance of such tests on sheet materials (ASTM D5420-98a, ASTM F736-95(2001)) and pipes (ASTM G14-88(1996)e1, ASTM D2444-99) (see their website www.astm.org).

The standard way of analysing the output of a dropweight machine assumes the weight behaves as a rigid body and hence that one can simply apply Newton's laws of motion. Thus in determining the calibration factor $k(N/V)$ of a dropweight force transducer dynamically, we assume we can replace $\int F dt$ by $m\Delta v$. Thus

$$k = \int F dt / \int V dt = m\Delta v / \int V dt, \tag{1}$$

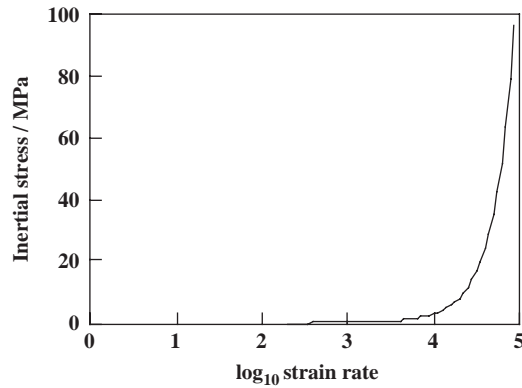


Fig. 3. Inertial stress as a function of strain rate calculated using the formula given in Ref. [4] for copper specimens 3.8 mm in diameter and 2.3 mm thick (the smallest specimen size used in Ref. [6]).

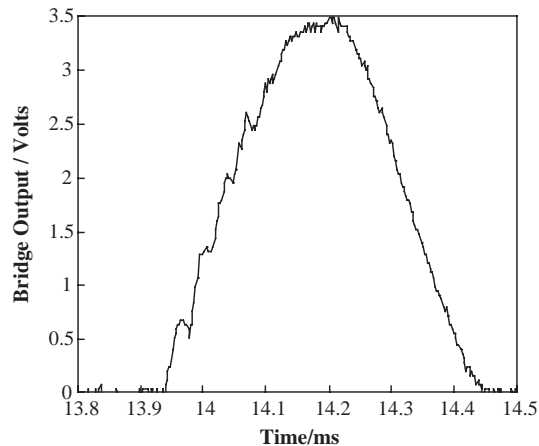


Fig. 4. Output of the strain gauge bridge for a dropweight force transducer calibration experiment.

where m is the mass of the dropweight, $\int V dt$ is the integral of the strain gauge bridge output voltage signal and Δv is the change of velocity of the weight produced by impact on the force transducer (remembering, of course, that velocity is a vector so that the magnitudes of the impact and rebound speeds must be *added*). A typical calibration signal is presented in Fig. 4. Dynamic calibration has been found to agree well with that performed statically in a calibrated commercial testing machine [16].

In practice, the output signal from a dropweight machine often has oscillations comparable in size to the signal produced by the mechanical resistance of the specimen. This is particularly true if the dropweight itself is instrumented, e.g. with accelerometers. The reason is that impact excites the weight below its resonance frequency [17]. Elastic waves, therefore, reverberate around inside until the momenta of the constituent parts of the weight have been reversed. Rebound then occurs and the specimen is unloaded. Recent work has demonstrated that it is possible to obtain high-quality data from such machines (at least for simple specimen geometries) either by the use of a

momentum trap in the weight if the weight itself has to be instrumented [18] or by careful design of a separate force transducer placed below the specimen [16].

Dropweight machines are also widely used in explosives safety qualification: the higher a standard dropweight has to be dropped onto an energetic formulation before half the drops produce ignition the safer that formulation is assumed to be [19]. One modification to the dropweight apparatus which has proved invaluable in the elucidation of explosives ignition mechanisms is to machine a light-path through the weight and to perform the deformation between transparent glass anvils [20–24]. This allows the event to be captured using high-speed photography. Examples of ‘classic’ high-speed photographic sequences obtained using this apparatus are given in Fig. 5.

3. Split Hopkinson pressure bars

Three researchers had the idea of using two Hopkinson pressure bars [26] to measure the dynamic properties of materials in compression [27–29]. Methods of obtaining high rate mechanical properties of materials in tension and torsion had previously been invented [30–33]. However, SHPBs were not widely used until the 1970s (Fig. 6). Instead alternatives such as the propagation of plasticity down rods or the cam plastometer [34] were used for obtaining dynamic mechanical properties in compression. As SHPBs increasingly became the standard method of measuring material dynamic mechanical properties in the strain rate range 10^3 – 10^4 s⁻¹, tension [35] and torsion [36] versions were developed.

The basic idea of the SHPB is that the specimen is deformed between two bars excited above their resonant frequency (Fig. 7). Note in comparing Figs. 4 and 7 the very different shapes and durations of the loading pulses. The material of the bars is chosen so that they remain elastic (small strains) even though the specimen itself may be taken to large strains. This means that strain gauges can be used repeatedly to measure the signals in the bars (strain gauges normally have small failure strains). Dynamic loading is produced either by striking one end of one of the bars (the input bar) or by statically loading a section of the input bar held at some point by a clamp and then releasing the clamp so that the load propagates to the specimen. Compression bars are nearly all of the dynamically loaded type (though there is no reason why in principle a ‘statically’ loaded compression SHPB could not be built). Tension SHPBs have been designed of both types [37]. Torsion SHPBs are nearly always statically loaded [38]. Tension and torsion systems have the advantage that friction between the bars and the specimen is not a problem. They have the disadvantage that the specimens are of more complex geometry and hence harder to fabricate. Also tension specimens usually have to a large length to diameter ratio so that issues of stress equilibrium and longitudinal inertia have to be carefully considered. Torsion specimens are usually thin-walled tubes which raises the issue as to how many grains or crystals they contain within the wall thickness and hence how representative they are of bulk material. One way round this is to shear simple discs of material of varying diameter [39] so as to be able to subtract off the mechanical effect of the ‘dead’ material in the centre. This requires perhaps 4–5 times as many experiments to be performed per data point, but the specimens, being simple discs, are much easier to fabricate than thin-walled tubes.

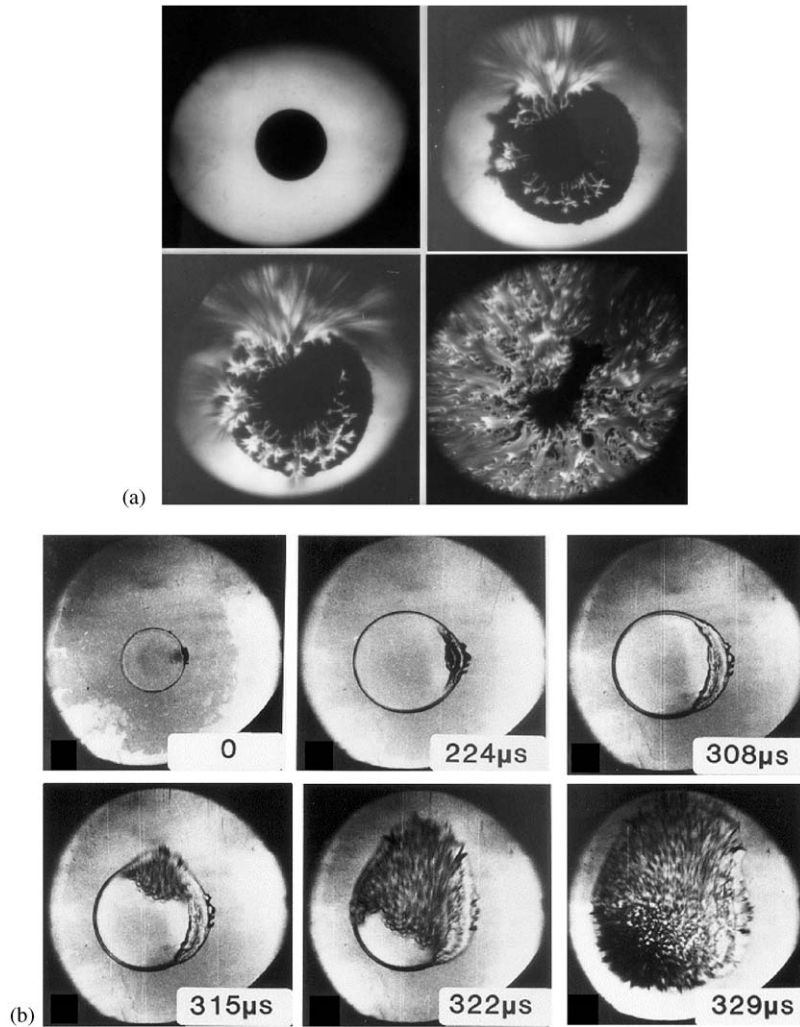


Fig. 5. Some ‘classic’ high-speed dropweight sequences. In both cases, the specimen was subjected to unconfined normal impact. (a) The ignition under impact of a thermite composition. Times from the moment of impact: 0, 329, 336, 420 μs . From Ref. [24]. (b) Deformation and fracture (unlubricated) of a 1 mm thick, 5 mm diameter polycarbonate disc. From Ref. [25].

The classic elastic wave analysis of the SHPB assumes that the rods are 1D objects (their true 3D nature is demonstrated by the oscillations on the recorded signals; see Fig. 7). The aim of the analysis is to relate the elastic strains in the rods (measured by, for example, strain gauges) to the force applied to and the deformation of the specimen sandwiched between them. The full analysis may be found in Ref. [40] and results in the following two equations:

$$\sigma(t) = \frac{AE\varepsilon_t}{A_s}, \quad (2)$$

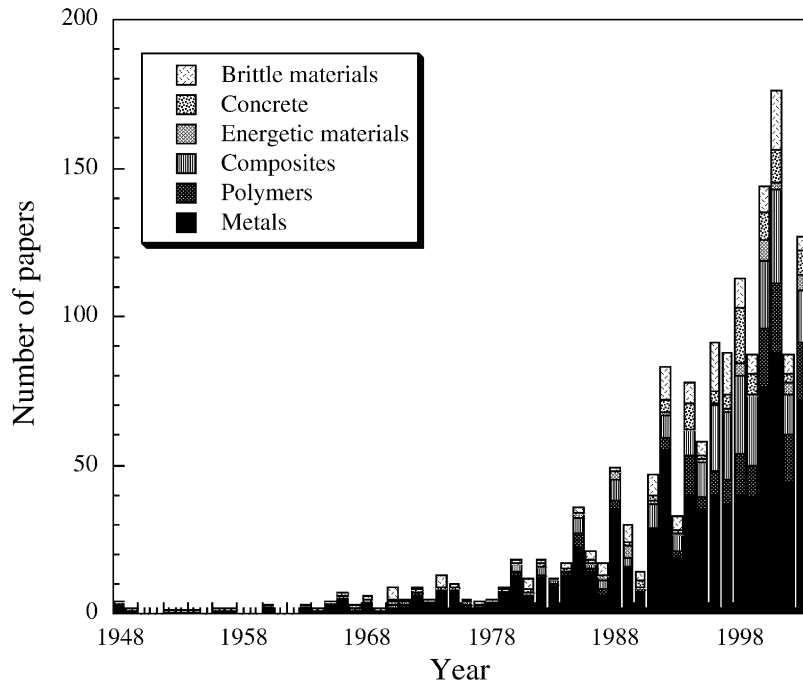


Fig. 6. Histogram of the number of papers published in any given year where an SHPB was used to obtain the high rate mechanical properties of various materials.

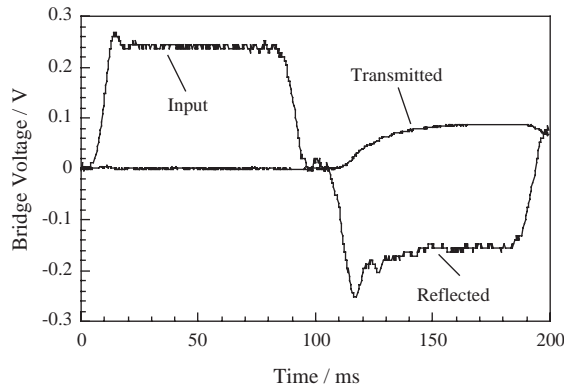


Fig. 7. Input (loading) reflected and transmitted pulses in a dural compression SHPB for a 4 mm thick, 5 mm diameter polycarbonate specimen.

$$\frac{\partial \varepsilon}{\partial t} = \frac{2c_b \varepsilon_T}{l_s}, \tag{3}$$

where $\sigma(t)$ is the stress in the specimen, A is the cross-sectional area of the bar, E is the Young's modulus of the bar material, ε_t is the strain pulse measured in the output bar (transmitted pulse),

ε_r is the strain pulse reflected from the specimen and measured in the input bar, $\partial\varepsilon/\partial t$ is the specimen strain rate, c_b is the elastic wave speed of the bar material and l_s is the current specimen length (thickness). The stress–strain curve of the specimen can be found from Eqs. (2) and (3) by eliminating time as a variable. Similar analyses exist for tension and torsion systems. Note that two major assumptions were made in deriving these equations: (i) the forces on the two ends of the specimen are the same, and (ii) the specimen deforms at constant volume. If either of these assumptions are false (which they are for foams, for example), the equations are invalid. However, the force–time data obtained may still be used for checking material models [41–43].

Fig. 6 shows that use of this method for obtaining high rate mechanical data started to become widespread in the late 1970s. Several groups of researchers have contributed to the development of the technique, summarised in Table 1. These modifications are driven by the desire to obtain data on a wide range of materials for impact modelling purposes but for which the assumptions made in deriving Eqs. (2) and (3) are suspect. Examples include polymer foams (for crash dummies) [44], metal foams (for blast mitigation) [45–47], polymer-bonded explosives [48,49] and semi-brittle materials such as concrete [10].

Fig. 2(a) is a ‘classic’ plot of the effect of strain rate on the mechanical properties of a ductile material, copper. This bilinear behaviour has also been seen in some polymers [91], but other polymers exhibit *drops* in flow stress above 10^3 s^{-1} [91,92]. This behaviour is still not understood [18]. The main problem in relating it to the loss peaks seen in dynamic mechanical analysis of polymers [93] is that the strains involved are very different.

We have recently investigated the effect of grain size on the high rate mechanical properties of an ammonium perchlorate (AP)/hydroxyl-terminated polybutadiene (HTPB) PBX [94]. This PBX consisted of 66% AP and 33% HTPB by mass. The AP was available in four different crystal sizes: 3, 8, 30 and 200–300 μm . We found that the effect of grain size was most clearly seen at low temperatures (Fig. 8). Fig. 9 shows that the effect of particle size on the flow stress of the material is linear in $1/\sqrt{d}$, where d is the particle size.

Table 1
Recent major developments in SHPB testing

Date	Development
1980	Gorham and Field develop the miniaturised direct impact Hopkinson bar [5,11]
1985	Albertini develops large SHPB for testing structures and concrete [50]
1991	Nemat-Nasser develops one pulse loading SHPBs (compression, tension and torsion) and soft recovery techniques [51]
1991–1993	Use of torsional SHPB for measurement of dynamic sliding friction and shearing properties of lubricants [52–54]
1992–2003	Development of polymer SHPB for testing foams [44,55–72]
1997–2002	Use of wave separation techniques to extend the effective length of a Hopkinson bar system [73–79]
1998	Development of magnesium SHPB for soft materials [48,80]
1998	Development of radiant methods for heating metallic SHPB specimens quickly [81,82]
1998–2002	Analysis of wave propagation in non-uniform viscoelastic rods performed [65,71,74,83–87]
1999	Development of one pulse torsion SHPB [88]
2003	Extension of Hopkinson bar capability to intermediate strain rates [89]
2003	Application of speckle metrology to specimen deformation [90]

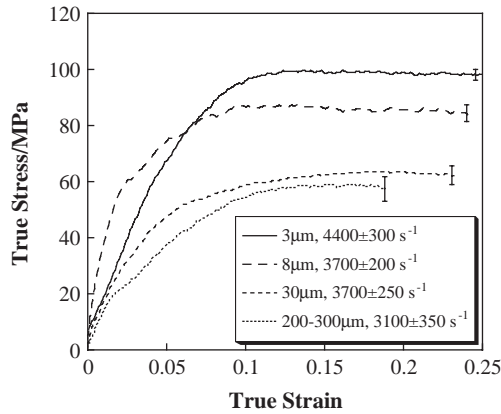


Fig. 8. Plot of the stress–strain responses of an AP/HTPB with four different AP crystal sizes at -60°C obtained using an SHPB. From Ref. [94].

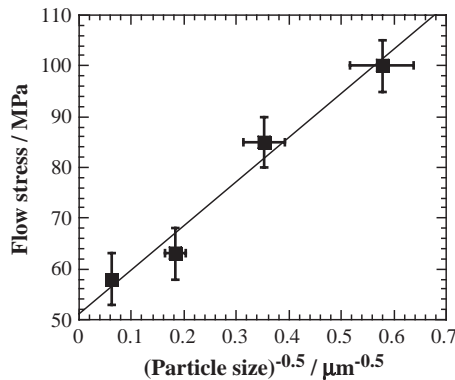


Fig. 9. Plot of the flow stress data of Fig. 8 versus the reciprocal of the square root of the AP crystal size. From Ref. [94].

Another ‘high tech’ application of SHPB techniques has recently arisen in the context of the failure of solder joints in mobile phones. In service, these are often dropped, and although the overall strain rate of the structure may be modest, very high rates of strain may be developed locally in the solder balls that form the connections between the various electronic components and the PCBs they are attached to. This is due both to the small size of the solder balls and the mechanical inertia of the components of the device. In order to model impacts on any structure, it is necessary to have a constitutive equation that represents the mechanical behaviour of the materials that make up that structure over the range of temperatures and strain rates of interest. In the case of mobile phones, the temperatures of interest range from the minimum found in the Arctic (say -60°C) to the maximum found in the Tropics (say $+50^{\circ}\text{C}$). Note from Figs. 10 and 11 the strong temperature and strain rate dependence of the mechanical properties of 63Sn37Pb solder material. Similar results have been found by other researchers [95,96].

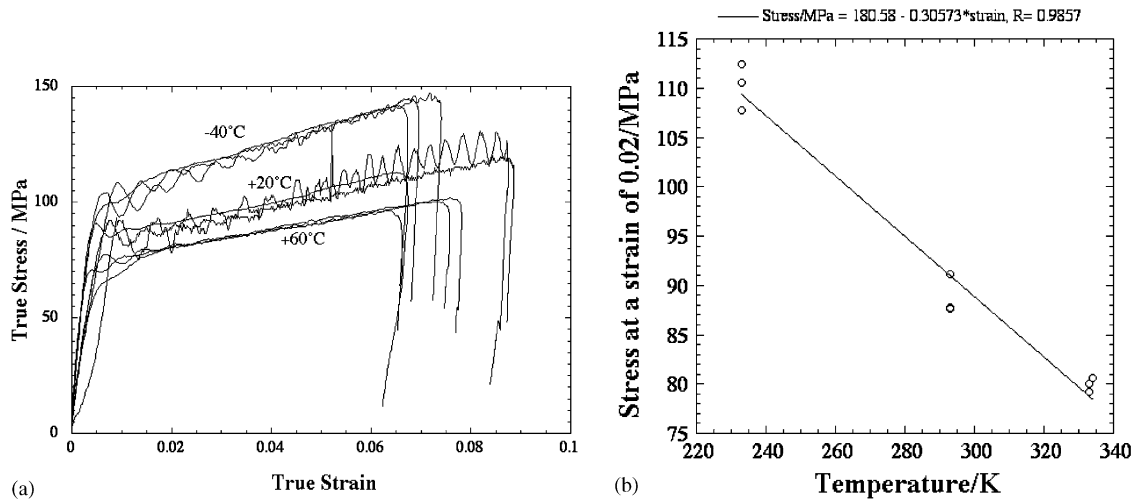


Fig. 10. (a) Stress–strain curves for 63Sn37Pb solder at strain rates of ca. 1000 s^{-1} and three different temperatures. (b) Plot of the stress at a strain of 0.02 versus temperature from the same data. From Ref. [97].

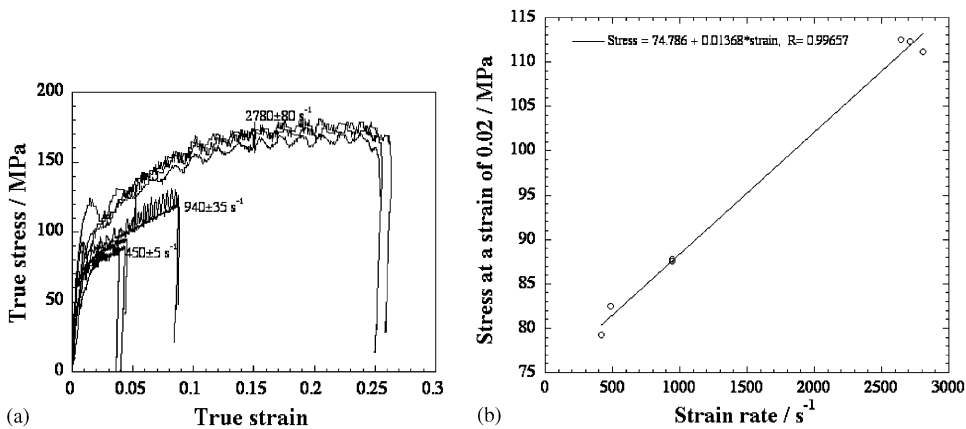


Fig. 11. (a) Stress–strain curves for 63Sn37Pb solder at three different strain rates at room temperature. (b) Plot of the stress at a strain of 0.02 from the same data. From Ref. [97].

With the increasing desire to obtain high rate data from materials for which the classic Hopkinson bar equations are not valid, alternative methods have to be used to obtain data from the specimen. For brittle materials, which usually fail before stress equilibrium is established, strain gauges have often been applied directly to the specimen [98–100]. This has a number of disadvantages: first, the gauge can only be used once; second, the gauge/bridge system must be calibrated in situ by statically loading the bar/specimen system in a calibrated machine; third, data can only be obtained from a few points on the specimen. A problem with foams is that they do not deform at constant volume until full densification has occurred. Hence, Eqs. (2) and (3) cannot be used to calculate the stress and strain. However, it is important to know their mechanical properties under impact as they are important energy absorbing materials in crash [101] and blast

[46]. Engineering stress–strain curves can be obtained assuming the foam deforms at constant area. Some make this explicit by using specimens of larger diameter than the bar [68]. Another problem that needs to be addressed is the large strain required before densification occurs. For any given strain rate (except the very highest), this is unlikely to occur within the time taken for one wave reflection within the striker bar. However, information about the continuing deformation of the specimen is contained within the waves that reverberate up and down the length of the bar system, and this information can be accessed with suitable analysis and software [68,73,75]. Another way of addressing this problem is to use the direct impact Hopkinson (or ‘block’) bar [102–104]. As with granular materials, the question may be raised as to how representative a foam specimen is of the bulk. This may not be such a severe problem for foams as evidence is accumulating that the mechanism of rate sensitivity is due to mechanical inertia of the cell walls so that even foams made from rate insensitive metals can exhibit substantially higher resistance to deformation under impact compared to quasi-static rates of loading [104,105]. Ideally high-speed or flash photography should be used when deforming foams or cellular materials so that the mechanisms of deformation may be identified.

Some optical techniques are particularly useful for these non-standard materials as they allow displacement data to be obtained from the whole of the field of view. One of the first optical techniques to be used in the SHPB was a diffraction grating ruled on the specimen [106]. However, this is an extremely time-consuming technique to use on a regular basis and requires very skilled technicians. J.F. Bell and his co-workers are the only ones ever to use this method. Speckle techniques are much easier to implement experimentally [107] but can require the implementation of complex algorithms and lengthy numerical calculations on a computer to obtain the displacement and strain fields [108]. Speckles can be formed by the interference of reflected coherent (laser) light from a surface [109] or by the application of spray paint (optical) [110] or fine smoke (for electron microscopy studies) [111]. Alternatively the microstructure of the material itself can be used if it is sufficiently granular [112]. In the last case, staining techniques may have to be used to increase the contrast between the various components. An example of the application of this technique to the deformation of specimens in a compression SHPB in our laboratory is shown in Figs. 12 and 13.

4. Taylor impact

The Taylor test was developed by G.I. Taylor and co-workers during the 1930s [27,114–116] as a method of estimating the dynamic strength of ductile materials in compression. The technique consists of firing a cylinder of the material of interest against a massive, rigid target. The dynamic flow stress can then be found by recovering the deformed cylinder, measuring its change of shape (Fig. 14) and using Eq. (4). However, this lacks the accuracy of deforming a disc of material and so Taylor impact is now rarely used for its original purpose. As mentioned before, a technique that is in some sense intermediate between Taylor impact and the SHPB was popular for about 25 years, namely the study of the propagation of plastic waves along rods, e.g. Ref. [117].

$$\sigma = \frac{\rho V^2(L - X)}{2(L - L_1)\ln(L/X)}. \quad (4)$$

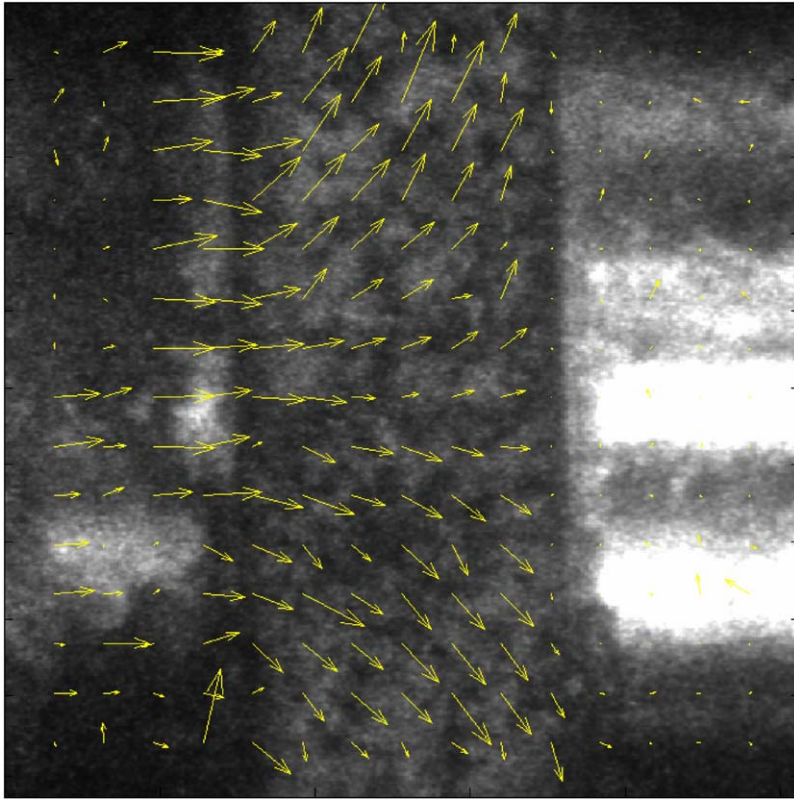


Fig. 12. Displacement quiver plots for an SHPB compression experiment on PBS9501. The length of the arrows is proportional to the displacement at their bases. Note that there are arrows on both the input bar and the specimen. From Ref. [90].

However, recently there has been renewed interest in Taylor impact or its variants (such as rod-on-rod impact [118]) as a method of ‘exercising’ constitutive relations [119,120] for a wide range of materials (see Fig. 15). High-speed photography is invaluable in these modern studies (see, for example, Figs. 16 and 17), and is essential for both brittle [121,122] and viscoelastic materials [123]. One reason this technique is so useful in exercising constitutive models is the wide range of strain rates it covers in one experiment from shock loading at the impact face to quasi-static loading at the rear [122,124]. It also produces large strains at the impact face.

5. Shock loading by plate impact

5.1. Shock physics

During the Second World War techniques based on high explosives were developed to produce planar shock waves in materials, principally metals [126]. Since then, a number of other techniques for shocking materials have been developed including high intensity lasers [127],

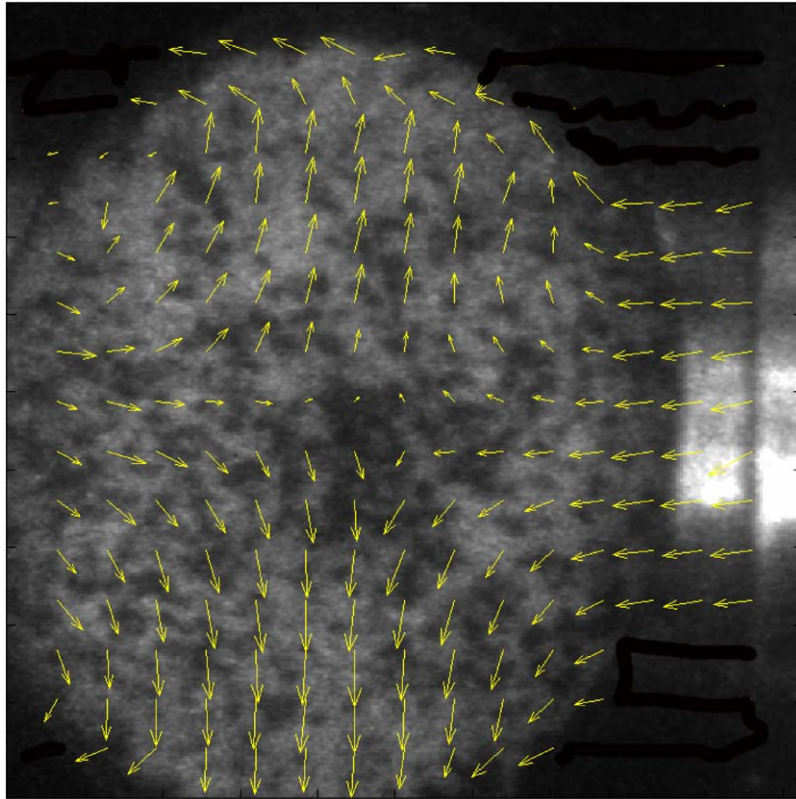


Fig. 13. Displacement quiver plots for a Brazilian experiment on PBS9501 in our SHPB. From Ref. [113].

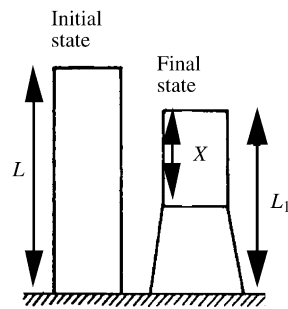


Fig. 14. Schematic diagram of initial and final states of a Taylor impact specimen. From Ref. [114].

nuclear bombs [128], particle beams [129] and plate impact [130]. Only the method of plate impact will be considered further in this review. The reader is directed to the several excellent review articles and books in the field for fuller information: Refs. [128,130–153].

In plate impact, the planar impact of a disc of material onto a target specimen (Fig. 18) produces shock waves in both target and impactor materials. The strain rate across a shock front is given by $u_p/U_s\tau$ where u_p is the particle velocity, U_s is the shock velocity and τ is the rise time of

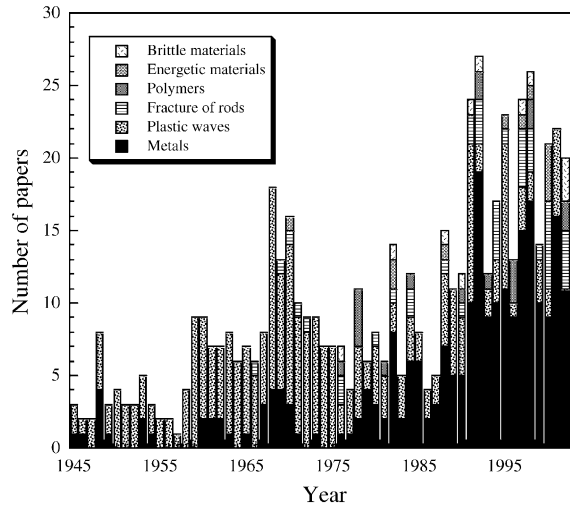


Fig. 15. Histogram of the number of publications published in any given year where Taylor impact or plastic wave propagation was used to investigate various materials.

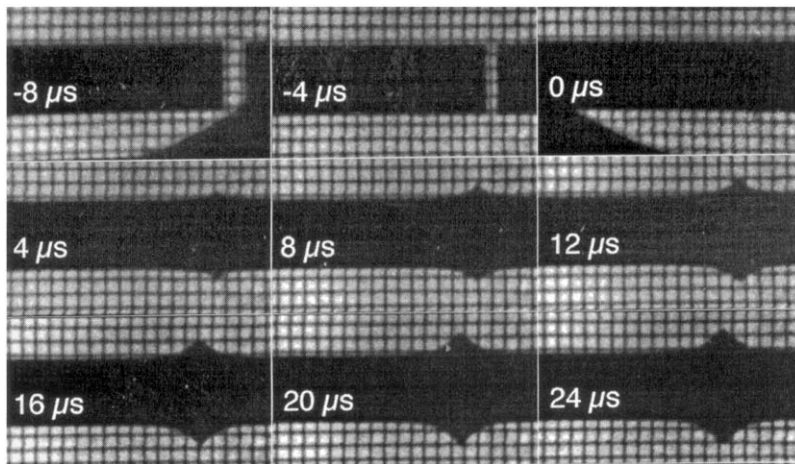


Fig. 16. Symmetric Taylor impact of 10 mm diameter, 100 mm long copper rods at 395 m s^{-1} . Stationary rod is on the left. Times are given relative to the moment of impact. The grid in the background has 2 mm squares. The triangular patches in the frames at -8 and 0 microseconds are the edges of the Imacon's fibre optic bundle. From Ref. [125].

the shock. Measured values of these parameters (u_p , U_s , τ) range from (0.1 km s^{-1} , 2.6 km s^{-1} , 50 ns) for polymers to (1 km s^{-1} , 10 km s^{-1} , 1 ns) for aluminas. These values give a strain rate range for materials swept by a shock wave from ca. 10^6 to 10^8 s^{-1} . These are the highest rates of deformation that can be achieved in the laboratory by mechanical means. As Fig. 1 indicates, deformation takes place at these strain rates under 1D strain. This is because the inertia of the material involved in the collision acts (for a period of a few microseconds) to rigidly constrain the material in the centre of the colliding discs. The loading, therefore, is 1D strain. This state of

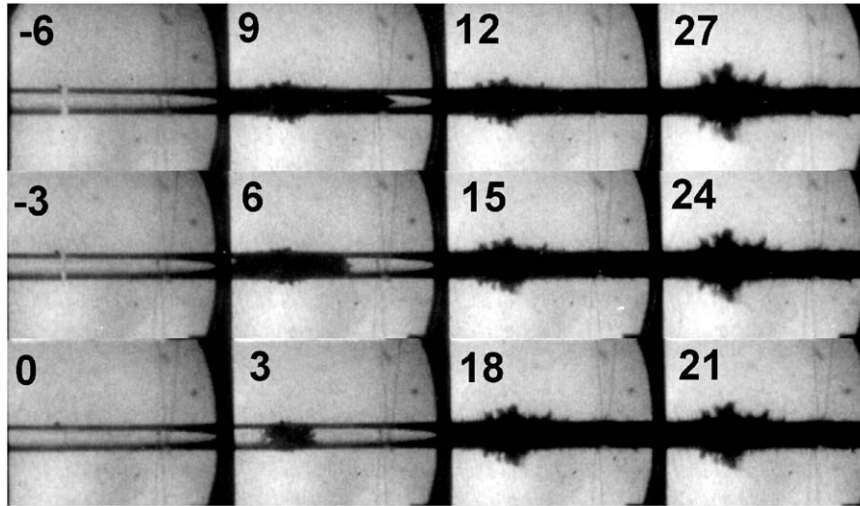


Fig. 17. High-speed photographic sequence of a symmetric Taylor impact using 10 mm diameter, 100 mm long soda-lime glass rods. Impact velocity 391 m s^{-1} . Numbers on frames are times in μs^{-1} before (negative numbers) and after (positive numbers) impact. From Ref. [122].

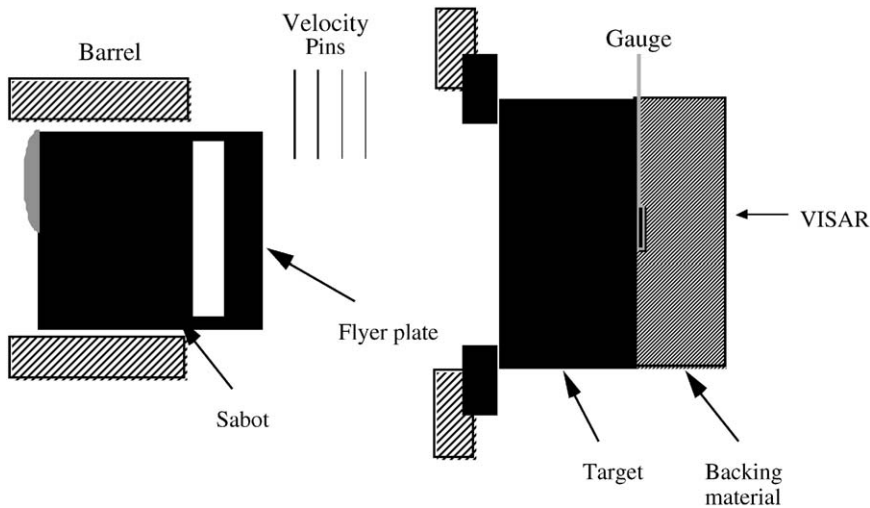


Fig. 18. Schematic diagram of the ‘business end’ of a plate impact shock loading gun.

affairs lasts until lateral release waves reach the centre of the discs, i.e. for a time given by r/c_s , where r is the radius of the disc and c_s is the appropriate wave speed in the shocked (and hence densified) material (see Fig. 19). Hence, the larger the diameter of the impactor/target the longer the state of 1D shock strain lasts for. However, the costs of manufacture and operation of a laboratory gun increase rapidly with the bore size. So most plate impact facilities use guns in the range 50–75 mm bore. Single stage guns operated with compressed gas have a typical upper impact speed of around 1.2 km s^{-1} if helium is used as the propellant. Higher velocities can be

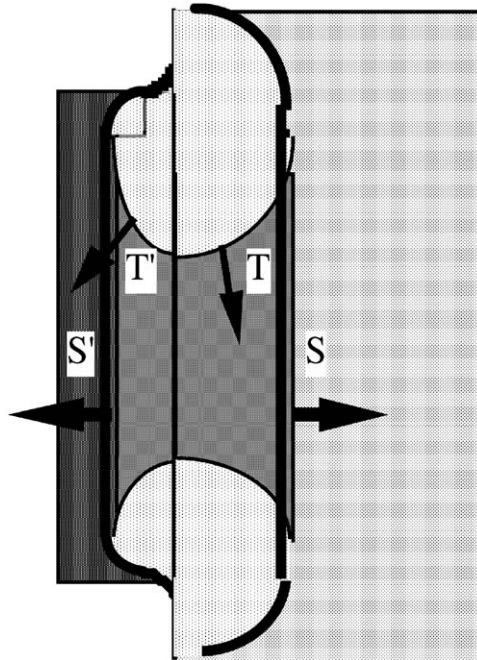


Fig. 19. Schematic diagram of the shock stresses in a plate impact just after the impact. Note the lateral release stresses labelled T propagating in from the edges. The shaded area in the middle indicates material in a state of 1D strain. This state lasts until the lateral release waves cross.

achieved with single stage guns using solid propellants, but this has the disadvantage of producing a great deal of residue which has to be cleaned out each time the gun is fired. To achieve impact speeds typical, say, of the impact of space debris on an orbiting satellite requires two- or even three-stage guns [154,155]. One disadvantage is that each successive stage is of smaller diameter than the one before. Hence, the final projectile is typically only a few millimetres in diameter. For the very highest speeds in such systems, hydrogen is used as the propellant.

Typical applications of the plate impact technique to materials include: (i) obtaining their Hugoniot curves (every material has a unique locus of possible shock states) [156]; (ii) measuring their dynamic spall (or tensile) strengths [157]; (iii) investigating high-pressure phase changes [158]; (iv) study of shock-induced chemistry [159]. Evidently, all of these are of interest to the military in applications such as armour, penetrators, shaped charges, explosives, etc., but there are many civilian applications as well including quarrying/blasting [160], shielding of orbiting satellites [161], geophysics [162], explosive welding [163], novel materials synthesis [159], etc.

5.2. Experimental techniques

A number of technologies have been developed in order to obtain data from shock experiments (Table 2). The electrical outputs of any gauges used must be sampled by oscilloscopes operating at 1 GS^{-1} or higher. High-speed cameras need to be able to operate at sub-microsecond framing rates in this application.

Table 2
Typical experimental diagnostics used in plate impact studies

Variable measured	Experimental technique
Longitudinal and transverse stress	Manganin, PVDF, ytterbium, carbon stress gauges
Surface strain measurements	Strain gauges, moiré with high-speed photography
Particle velocity	VISAR, particle velocity gauges
Spall strength and dynamic compressive strength measurements (HEL)	Manganin or PVDF stress gauges, VISAR
Wave structure in transparent materials	High-speed photography/stress gauges
Temperature	Spectroscopy, pyrometry

Whilst we predominantly use manganin stress gauges in our laboratory, given their extensive calibration [164,165], there are several other types available. A candidate gauge material needs to satisfy the following conditions: (i) high sensitivity to pressure; (ii) low sensitivity to temperature; (iii) stable resistance with time; (iv) low sensitivity to composition and manufacturing techniques; (v) linear (or very nearly so) response to pressure; (vi) no phase transitions in working pressure range.

Manganin fits all of these requirements but ytterbium [166,167] and carbon [168,169] are used in low stress regimes and in some explosive work [170] even though they do not meet several of the requirements listed above. Piezoelectric gauges have been used for many years and a wealth of literature exists on their polarisation under shock. The most investigated of these materials are quartz, PZT and lithium niobate [171–174]. Recent interest has centred around poly(vinylidene difluoride) (PVDF); a piezoelectric polymer [175,176]. Such piezofilms are of interest as potential gauge materials since they have high output and offer the opportunity of dispensing with power supplies. At present the response of these gauges is limited by the thickness of the film to ca. 100 ns. These gauges can be used in one of two different configurations denoted charge mode and current mode. In the former, the gauge sees a charge integrator and the output can be sent directly to an oscilloscope to measure a voltage proportional to the stress. In the latter, a current viewing resistor is placed across the gauge and the voltage across it is monitored directly. In this case, the stress derivative is measured and a time integration must be carried out to recover the stress signal. It is this latter method which is generally favoured because of the bandwidth problems of hardware integrators. We have manufactured our own gauges and have simultaneously measured wave profiles in ceramics with both manganin and PVDF gauges with good results [177]. In Fig. 20, typical gauge records are shown taken with manganin (solid line) and PVDF (dotted line). The gauges were placed next to one another in polymethylmethacrylate (PMMA). The target was a ceramic with a very rapidly rising elastic pulse impacted so as to achieve a stress of ca. 0.5 of the dynamic compressive strength (Hugoniot Elastic Limit, HEL). Note the relatively longer rise time for the PVDF and the discrepancy in the PVDF reloading signal which needs further investigation.

Rather than using gauges, many laboratories have chosen instead to develop velocity interferometry to measure the free (usually rear) surface velocity of the target. This velocity can be related via the shock impedance to the induced stress and the stress–time history can thus be inferred. The most versatile instrument of this type is the velocity interferometer system for any reflector (VISAR) [178] which dispenses with the need to have a reflective rear surface thus

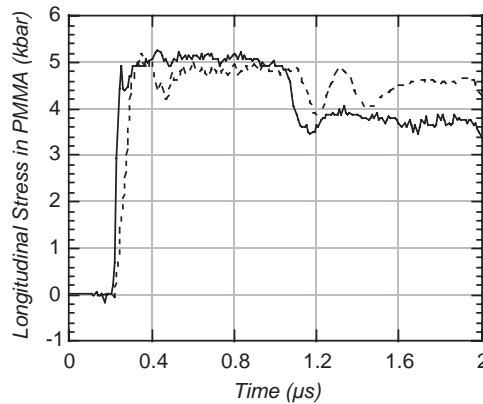


Fig. 20. A comparison of manganin (solid line) and PVDF (dotted line) gauges. In both, 3 mm aluminium flyer impacting at 270 m s^{-1} on a ceramic with very fast rising compression pulse. From Ref. [177].

allowing measurements to be taken on deforming surfaces. Normal and transverse velocity interferometry are necessary to determine the behaviour of materials at high shear strain rates in the so-called pressure–shear configuration [179,180]. In our laboratory, we use both gauges and VISAR since these both optimises and cross checks the data obtained.

It is important to be able to relate the measurements made in plate impact, an idealised laboratory technique, to what happens, say, in real ballistic impact where the triaxial strain state set-up in the material lies somewhere between uniaxial strain and uniaxial stress. It has been found that the shock shear strength controls the ballistic performance of target materials [181]. A direct and fully experimental method of measuring this parameter is to record both the longitudinal and lateral stresses using thin piezoresistive gauges [182]. The dynamic shear stress is then given by half the difference between the longitudinal and lateral stresses (Fig. 21). In order to account for the response of the lateral gauge a careful analysis of its loading and unloading characteristics is needed [183].

5.3. Brittle materials: ceramics and glasses

Why are shock experiments performed when real impacts create 3D states of strain? The main purpose is to use the shock wave as a probe, first to introduce damage (and compaction if the ceramic is porous) in a controlled manner and then to study the resulting damage [185–187]. Such damage studies cannot be done by quasi-static high-pressure diamond-anvil compression studies. Shock-wave experiments are a precise and orderly method of subjecting a material to carefully controlled compression [132]. From a theoretical (modelling) point of view, the 1D situation must be understood before the 3D case can be tackled. Experimentally, it is extremely difficult (if not impossible) to instrument a specimen subject to a fully 3D ballistic impact loading and obtain meaningful data [188]. It is, therefore, necessary at present to try and relate the properties obtained in a 1D shock experiment to those relevant to ballistic impact.

Brittle materials have a variety of responses to shock: some are relatively undamaged by shocks above their HEL, others fail immediately the HEL is exceeded. However, contradictory results

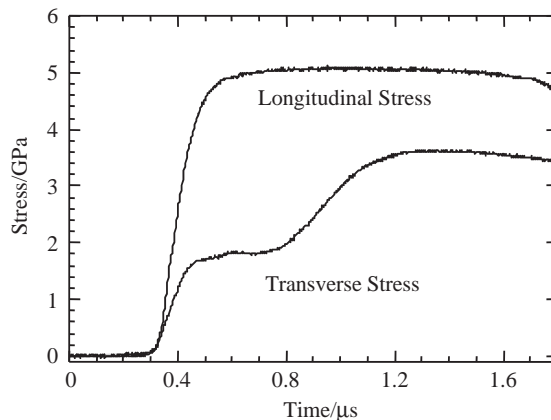


Fig. 21. Illustration of lateral and longitudinal gauge signals showing change of shear strength of float glass ca. $0.4 \mu\text{s}$ after the impact. From Ref. [184].

have been published for the same materials, some authors claiming, for example, that pure alumina shows compaction but no sign of fracturing even when shocked to twice its HEL [189] whereas Rosenberg and Yeshurun [190] demonstrated a reduction in spall strength for alumina shocked to only half of the HEL. Double shock techniques can allow these sorts of controversies to be resolved as it uses one shock to damage the material and a second shock immediately following to probe the state of the shocked material, particularly the shear and spall strength [185]. Rosenberg et al. [191] concluded that the HEL marks the point at which cracks coalesce into a network. Borosilicate glass was shown to exhibit no loss of spall strength up to the HEL and then a substantial loss of shear strength when shocked above the HEL [192]. Soda-lime glass, on the other hand, showed a finite (though reduced) shear strength [193]. This loss of shear strength was correlated with a sudden increase in penetration depth at a certain critical impact speed [194] when glass specimens were struck by flat ended projectiles.

A stir was caused in the Shock Physics community when some Russian researchers showed that failure in shocked glass propagates *behind* a compressive shock [195,196]. This was detected as a smaller reload signal in the shock wave (recorded using VISAR) than would be expected if spall had taken place in previously undamaged material. It was a small effect, but it was enough to alert them to the presence of a region in the material with a slightly lower shock impedance than the original material. Since the shock wave had had time to reflect off the back surface and be partially reflected off this zone of lower impedance, the failed zone must have been propagating more slowly than the shock-wave velocity.

This paper resulted in a number of studies being carried out into this phenomenon in a variety of laboratories, including ours. High-speed photographic sequences of failure fronts were obtained in our laboratory [197,198] (see also Figs. 22 and 23). (Note that some researchers use the expression ‘failure waves’, but we regard the word ‘wave’ as inappropriate as the propagation is not described by a wave equation.) As the shock pressure is raised, the gap between the failure front and the shock wave is found to decrease, reaching zero at some critical impact shock pressure [199]. This immediately raises the issue of kinetics of damage (discussed in more detail below). It should also be emphasised that failure fronts are only detectable photographically when

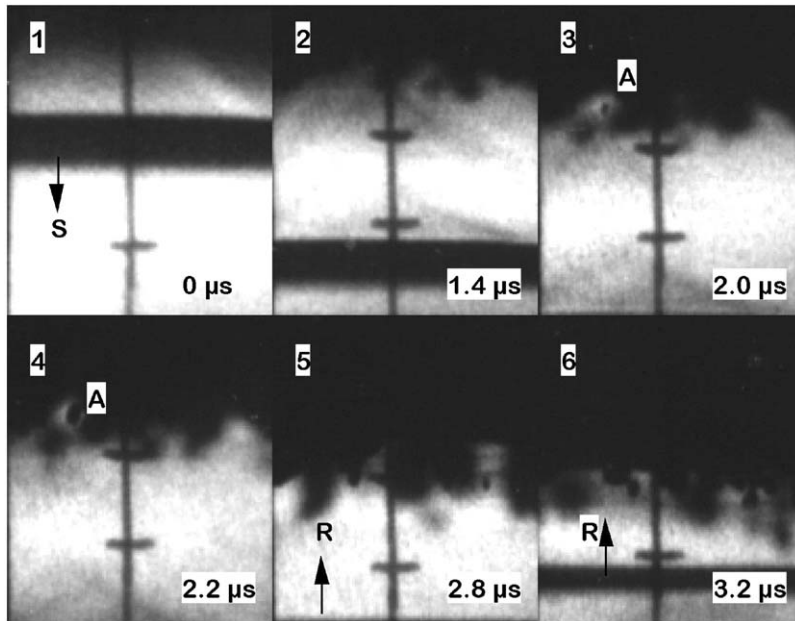


Fig. 22. Soda-lime glass impacted from the top at 250 m s^{-1} . A shock S travels down through the frames, leaving in frame 2. The scale markers are 5 mm apart and the first is 15 mm from the impact face. A failure front appears behind in frame 2 and a damage site, A , nucleates and grows in frames 3 and 4. The reflected release R from the free surface enters the frame from below in frames 5 and 6. The exposure time for each frame is 50 ns. From Ref. [197].

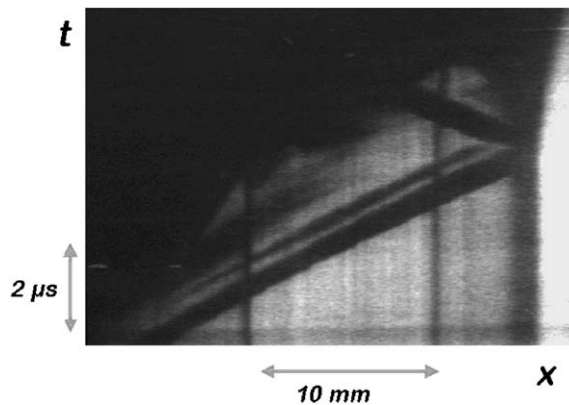


Fig. 23. Streak photograph of shock and failure front in soda-lime glass shocked by plate impact at 533 m s^{-1} . From Ref. [198].

the fracture face separation is greater than $\lambda/2$ (where λ is the wavelength of the illuminating light). Gauges may be useful here in detecting loss of shear strength in the material in the transparent region between the shock wave and the failure front.

Failure fronts have also been sought in other brittle materials [200,201], although the evidence for their existence in materials apart from silica glasses is still controversial. Some researchers

claim that in some brittle materials (such as alumina) failure does not propagate very far into the material from the impact surface [202–204], although others claim this may be a measurement artefact [205,206]. A few researchers have linked failure fronts to resistance to ballistic or hypervelocity impact [201,207–209].

One important consequence of the discovery of the failure front phenomenon has been to highlight the importance of including kinetics in ceramic (or at least glass) failure models. Any constitutive damage model that assumes the material transitions instantly from an undamaged to a damaged state is clearly wrong. The main fragmentation models in the literature are those due to Mott [210,211], Grady and Kipp [212–218], Johnson and Holmquist [219–221], Clifton [222] and Steinberg and Tipton [223]. Mott originally developed his model during the Second World War for the explosive fragmentation of shell cases. Grady and Kipp also had this problem in mind when they developed their model, but they also applied it to a variety of problems including fracture of oil shales (and other rocks) and armour ceramics. The Johnson–Holmquist model was developed primarily for armour ceramics [221].

The main feature of the Grady–Kipp model relevant to shock loading and subsequent failure of ceramics is the postulate of the existence of a dynamic failure surface lying *above* that determined quasi-statically (Fig. 24). The position of this upper surface is independent of the position of the lower (quasi-static) surface. An implicit assumption is that the position of the HEL of brittle materials is a manifestation of fracture kinetics. Hence, it should be strain rate dependent. Evidence for this has been presented in terms of elastic precursor decay for various ceramics, e.g. Refs. [224–227], although doubts have recently been expressed about this interpretation of the data [206]. Anyway, Grady is on record as saying [215,216] that in some circumstances the older model of Mott [210] is superior to his own.

The main problem with the existing models is that they say nothing about how or by what path the material goes from the undamaged to the damaged state. Some sort of history-dependent model is required, and there are some groups working on this problem at the present time, e.g. Ref. [124]. For these reasons, it is probably not worth discussing the various existing failure models in depth in this review.

An interesting observation to end this section on is that due initially to Bourne and co-workers [230,231]. They found that the failed and unfailed shock shear stresses of glasses of widely

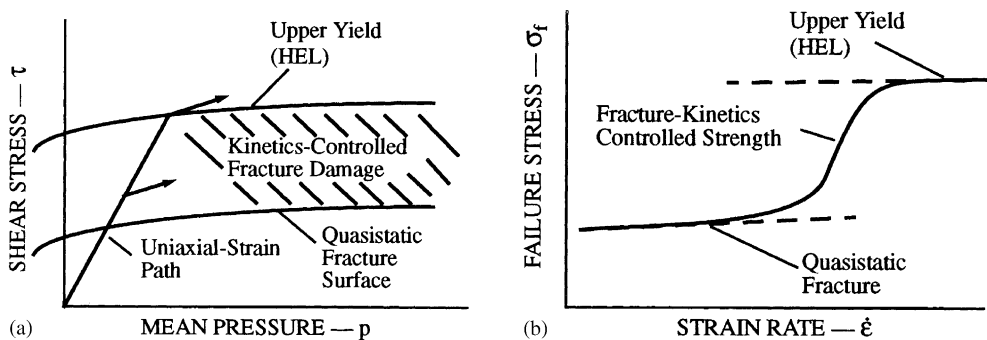


Fig. 24. (a) Schematic diagram of the Grady–Kipp model applied to shock loading and failure of brittle materials. (b) Consequences for kinetics of failure and position of HEL. From Refs. [228,229].

differing densities lay on the same curves (Fig. 25). Note these data have *not* been scaled or normalised. The origin of this unexpected behaviour is still uncertain, but must lie in what they have in common: a random network of silicon dioxide tetrahedra. In that figure, the data are compared with two other brittle materials. One important aspect of this phenomenon they missed, however, is the pressure dependence of the shear stress of the failed material (Fig. 26) [232]. This is simply because they did not perform experiments at high enough shock stresses (it would be expected that a comminuted material, mechanically similar to sand, would obey a pressure-dependent Mohr–Coulomb yield criterion). The strength of the failed material initially decreases, but with increasing longitudinal stress σ_x , the interlocking fragments exhibit a greater resistance to

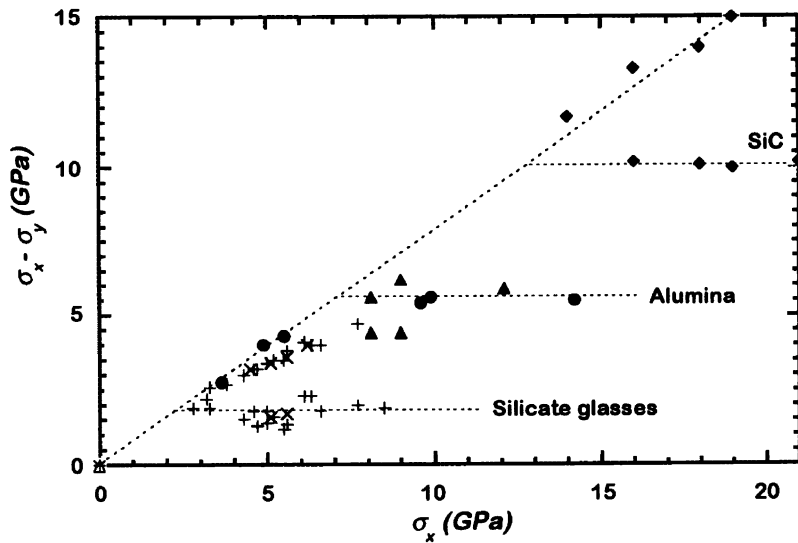


Fig. 25. Variation of the shock shear strength of three different brittle materials in the failed and unfailed states. From Ref. [230].

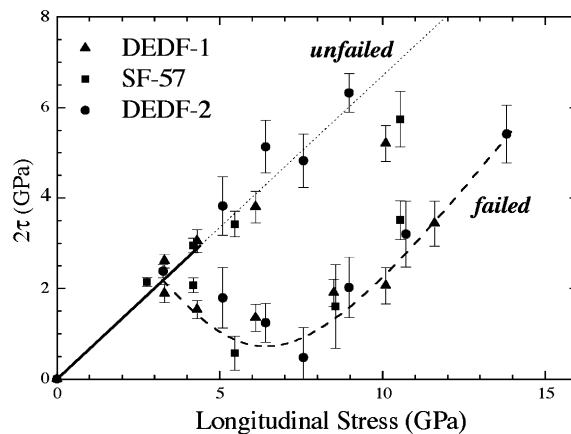


Fig. 26. Deviatoric responses of dense glasses tested up to ca. 14 GPa longitudinal stress. From Ref. [232].

shear, which is important to the ballistic response. Recent reviews of the failure front phenomenon have been written by Brar and Espinosa [233] and Brar [200]. The problem remains of interest to theoreticians of fracture mechanics [234,235].

Because of comminution, the relationship between ballistic performance and materials properties is very complex for brittle materials. Different materials and armour constructions may be needed to defeat different threats. For small arms fire, the full strength of a ceramic tile can only be exhibited if the tile is heavily confined and rigidly backed so that flexural failure cannot occur. If in addition the tile is large, it will not be penetrated by a projectile if

$$0.5\rho_p V^2 + Y_p \leq R_t, \quad (5)$$

where Y_p and R_t are strength parameters characterising the projectile and the armour, respectively [236–239]. Thus, only a thick backing technique can differentiate between different ceramics [190,240,241].

\bar{Y}/ρ has been found to be a true figure of merit with this technique for small arms ammunition [242]. B_4C is the ceramic that performs the best in this test against 0.3'' (7.6 mm), 0.5'' (12.7 mm) and 14.5 mm rounds. However, for long rod penetrators the situation is very different. This ammunition is made either from tungsten alloys ($\rho_p = 17,800 \text{ kg m}^{-3}$) or depleted uranium ($\rho_p \approx 19,000 \text{ kg m}^{-3}$) and impacts at 1.4–1.6 km s^{-1} , compared to steel bullets which move at 800–900 m s^{-1} . Thus, $\rho_p V^2/2$ is very large for long rod penetrators so that $\rho_p V^2/2 + Y_p \geq R_t$ (Y_p is the same as for hard steel, i.e. ca. 20 kbar) and penetration does occur (alongside rod erosion). Rosenberg and Tsaliah [239] were the first to demonstrate that Tate's model for steady-state penetration of ductile (metallic) materials [236,237] holds also for ceramics in which rod erosion also occurs. They found values of R_t (resistance to penetration) which compared well with those calculated by Forrestal and Longcope [243] for ceramic materials.

Shockey et al. [244] and Curran et al. [245] have tried to answer the question: which is the most important parameter to describe the penetration resistance of comminuted material? They claimed that friction (which is pressure dependent) is the most important; see also Refs. [246–248]. But this is similar to the suggestion of Rosenberg and colleagues that the shear strength (also pressure dependent) is the most important parameter. That was why they developed the lateral gauge technique since if you can measure the lateral stress σ_y you can obtain the shear stress experimentally as a function of pressure $\tau(p)$ (pressure is proportional to σ_x) from the identity $\tau \equiv (\sigma_x - \sigma_y)/2$. They found this parameter varies from ceramic to ceramic and correlates with ballistic performance [249,250]. Alumina and aluminium nitride were found to exhibit 'elasto-plastic' behaviour [251] whereas TiB_2 exhibits pressure hardening [252].

Glass, on the other hand, shows a loss of shear strength even below its HEL [232] (Fig. 26). This is similar to what we expect for B_4C because there is a very large difference between its elastic and 'plastic' wave speeds [253,254]. For TiB_2 , on the other hand, the two waves are almost indistinguishable [252]. On our present understanding, these features correspond with the long rod ballistic performance of these materials making TiB_2 one of the best in these applications while B_4C and glass have very low R_t values, presumably because of their loss of shear strength at high shock pressures. Thus B_4C , which is the best against small arms fire, is one of the worst against long rod penetrators (as is glass). However, glass is excellent against shaped charges because of its bulking which acts to disrupt the jet: the 'pinch' effect [255]. The conclusion is that it is not

possible to pinpoint one materials property that will give the ballistic performance against all threats.

Shock-wave experiments give the HEL and the shape of the Hugoniot, whether it is elasto-plastic, pressure hardening or pressure softening. Also the release part of the signal tells you how much strength remains in the shocked specimen by how far the release curve is from the hydrostat. Measurements of the lateral stress σ_y gives you the pressure dependence of the shear strength directly [182,232]. The challenge now is to measure it for the released material and not only at the peak pressure. This is what Klopp and Shockey [256] claimed to have measured. A recent comparison of the shock properties of various armour ceramics has been published by Fujii et al. [257].

In summary, the following points still have to be addressed in relating the properties measured by plate impact to ballistic impact on ceramic armours:

- (i) What is the meaning of the HEL of brittle materials in terms of damage level [205]?
- (ii) What governs the decay of the elastic precursor in those ceramics that exhibit this phenomenon [206]?
- (iii) How does the shear strength of a shocked specimen affect its ballistic resistance [250]?
- (iv) How can the magnitude of the shear strength *during unloading* be calculated from the experimental data?
- (v) What is the nature of the failure front? Is it a phase change as Clifton has suggested [222]; see also Ref. [200]? Related to this are the kinetics of the transition to the failed state. High-speed photography shows what appears to be a fracture front propagating behind the shock, but photographs need to be interpreted with care [122,231].
- (vi) What sort of 2D experiments should be performed to measure the dynamic properties of failed ceramics (or confined sand) which might be more relevant to their ballistic behaviour? Recent developments in X-ray speckle techniques are proving particularly exciting here [258–266].

5.4. Combined experiment and modelling of metallic systems

Being a uniaxial strain method, the shear strength of the material governs the shape of the loading and unloading part of the shock wave. As well as the yield strength under uniaxial strain, quantitative values for the spall (tensile) strength can also be obtained. By using plates of different fractions of the thickness of the target, the spall strength of material at differing positions behind the shock wave can be probed. This works because the thickness of the flyer plate controls the time at which the overlap between the two unloading waves reflected from the rear free surfaces of the target and the flyer occurs (see Fig. 27a). The reload signal (Fig. 27b) is a measure of the spall strength σ_{spall} .

Spall strengths have been measured in many materials. The variation in value as a function of the initial shock input [267] and the incipient formation of the spall plane [268] have been studied. Modelling of such systems is non-trivial and requires the successful integration of several steps; the passage of shock waves through an uncompressed material, the dispersion of the release waves (the so-called ‘release fans’), the interaction of the releases and the fracture limit [269–279].

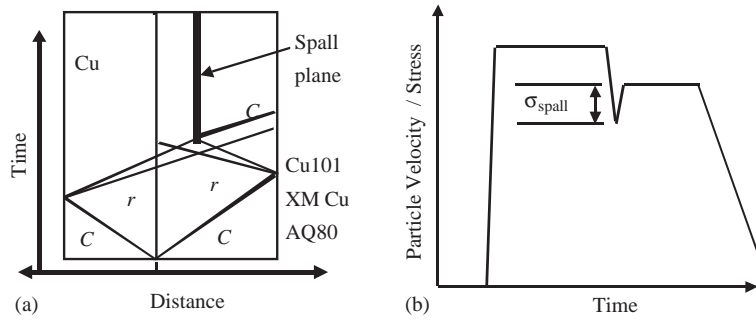


Fig. 27. (a) Wave propagation diagram, C = compression wave, r = release fan, (b) schematic diagram of corresponding velocity of rear of target plate.

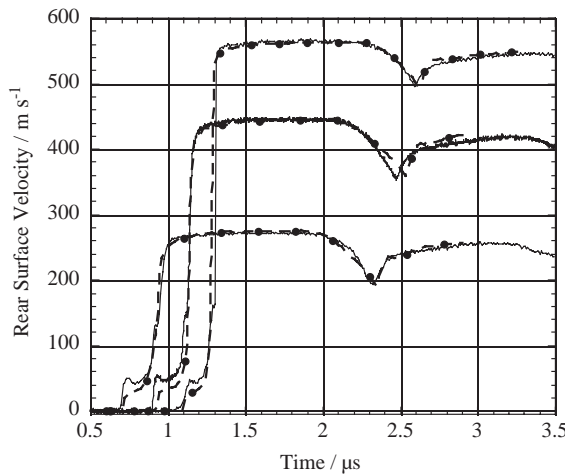


Fig. 28. The spall traces of AQ80, impacted at 256, 461 and 585 m s^{-1} . Solid lines are experimental data, hatched lines with markers are the model. From Ref. [272].

Recent work has used VISAR to obtain data on the spall strength of iron and selected copper systems and the results modelled using a Lagrangian hydrocode, DYNA-2D, which incorporated the Goldthorpe path-dependent ductile fracture model [280]. The advantage of the use of VISAR is that it provides high-time resolution ~ 2 ns data and can average over large areas of surface. The results of combined experiment and modelling are shown in Fig. 28.

It is crucial to perform the simulation with accurate constitutive data for both target and flyer plates. Whilst this is obvious for the target plate, it is not so obvious for the flyer. An illustration of the sensitivity of these results is shown in Fig. 29 where the higher velocity experiment has been simulated using an elastic plastic model for the copper flyer and literature data for the elastic properties. Although the comparison is fair, there are some significant differences relating to subtleties in the release fan from the back of the flyer plate. This reinforces the view that great care is required in simulating plate impact spallation tests.

Research in many American national laboratories currently concentrates on the effect of mesoscale structures on the signal. Line imaging VISAR has been used at resolution sufficient to

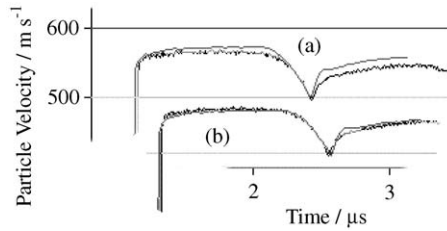


Fig. 29. Effect of release from flyer plate using (a) literature values, (b) parameters measured on the flier before use. From Ref. [272].

observe the motions of individual grains. This approach is complex and requires the use of sophisticated models and supercomputers. Such measurements are currently not proven to be of practical use but may be of greater versatility in the future.

Many other materials have been studied under 1D shock loading conditions in plate impact facilities. Indeed, if it is physically possible to place the material at the end of a gun, someone somewhere is likely to have shocked it! Major classes of materials not covered in this review, but which have been and are much studied, include polymers, energetic materials (such as explosives), granular materials (such as sand), rocks and concrete, ice, etc. Around 14,000 papers have been published on this topic on all classes of materials since the 1940s.

6. Reverse ballistics studies

Scientific ballistics studies require a great many variables to be measured simultaneously. Such experiments fall into two basic types: (i) normal ballistics where the projectile, such as a rod or cone of material, is fired at an instrumented target and (ii) reverse ballistics in which a target, such as a plate is fired at an instrumented 'projectile' [281,282]. One advantage of reverse ballistics studies is that many instrumentation techniques can be applied to the system that may be difficult or even impossible to use in normal ballistics. There are advantages also in studying scaled-down systems as the expense of an extended study on full-size targets and projectiles is generally prohibitive.

Many long rod penetrator systems are based around tungsten alloy rods [283–285]. So in the studies summarised here tungsten alloy rods were impacted by RHA plates in a reverse ballistic impact geometry. The data gathered from instrumented rods can be used to validate models used in ballistics codes [282,286–290]. Previous work performed in our laboratory concentrated on rod/plate interaction at fixed angles of 45° or 60° [291]. That research was extended to include the use of various high-speed diagnostic techniques [3,292] with particular emphasis on the effects of pitch [282].

The experimental arrangement and the definitions of positive and negative pitch are shown in Fig. 30. The tungsten rods used were 6.0 mm in diameter and 90.0 mm long. Each rod had two constant and foil gauges (EA-06-031CF-120, Micromasurements, Basingstoke, UK) mounted approximately one rod diameter from the impact face. The gauges were powered by a constant current supply which was adjusted to give minimum ringing for a response time of ca. 10 ns. The

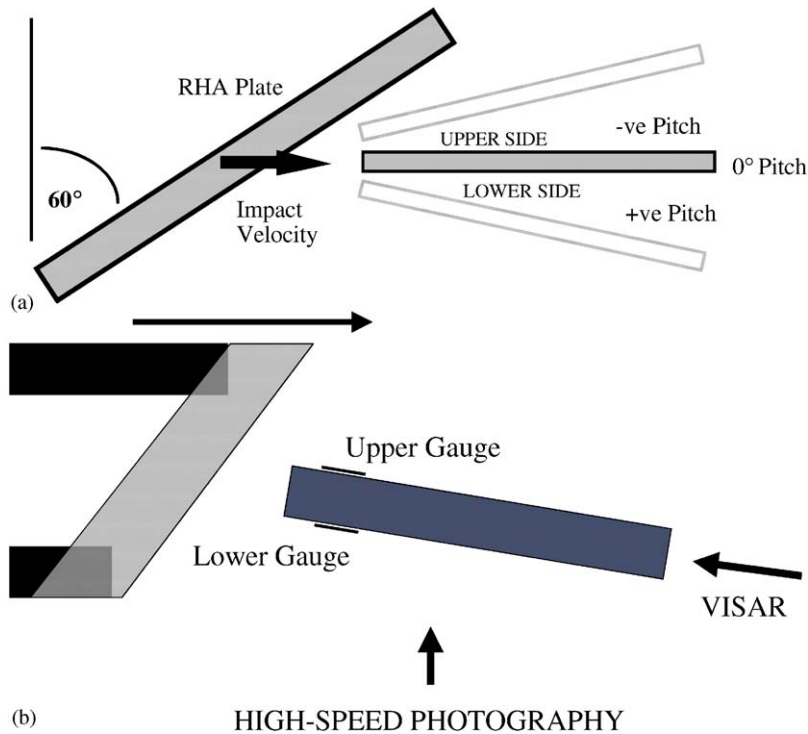


Fig. 30. (a) Experimental layout for reverse ballistic impact and (b) arrangement of diagnostics.

active length of these gauges is 1 mm, so since the sound speed in tungsten is ca. $3.8\text{--}4.0\text{ mm }\mu\text{s}^{-1}$, their response time is ca. $4\text{ }\mu\text{s}$. Compression reduces the gauge resistance and gives a negative signal while tension tends to increase the resistance and results in a positive signal. The motion of the tail of each rod was recorded using VISAR [178,293]. Laser light is reflected from the surface of interest and the reflected light is fed into the interferometer system. The fibre optic used for the VISAR was held in a holder ca. 10 mm from the rod tail. The velocity was thus measured *normal* to the rod's rear surface. High-speed photographic sequences were taken of the impact events using an Ultramac FS501 image converter camera in conjunction with a Bowen flash.

In Fig. 31, gauge outputs are presented for variation of the pitch in 3° steps. In these traces a very obvious trend is found which indicates the differing nature of the mechanisms involved. At high negative pitches, the lower gauges show a rapid rise to high levels of strain while the upper gauges show a slow rise to much smaller compressive strains. At positive pitches, it is the upper gauge trace which rises slowly, while the lower gauge rises rapidly. This implies that at negative pitches the rod tends to bend away from the target whereas at high pitches the rod tends to bend towards the target.

Two features that need much closer examination are the general humped nature of the lower traces, where the strain rises then falls close to zero. The traces from the upper gauges show a plateau, especially at 0° and $+6^\circ$. These would seem to relate to flexing during the penetration.

Overall a negative pitch tends to favour a sliding action followed by penetration through the plate, while positive pitches tend to favour an immediate cutting action into the surface. These

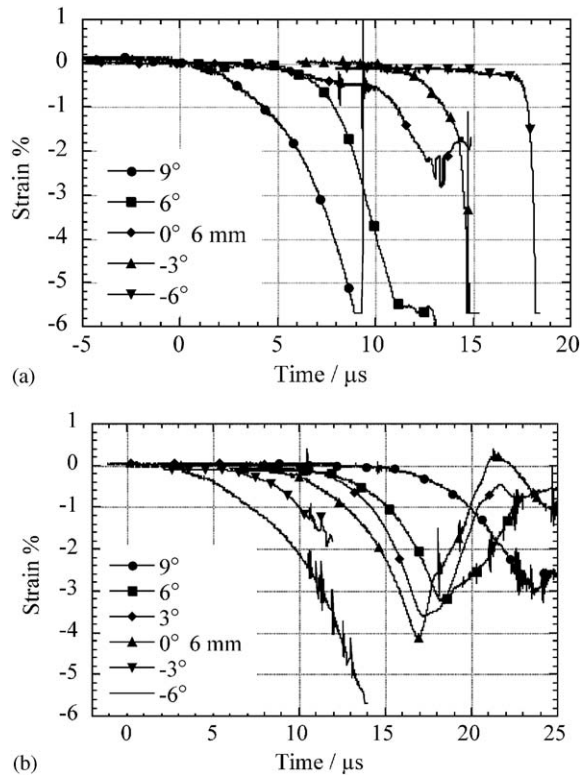


Fig. 31. Comparison of strain outputs from gauges on (a) upper side and (b) lower side of tungsten rod during impact. From Ref. [282].

penetration mechanisms are what could be expected given the initial angle of contact between rod and plate as emphasised in Fig. 32. However, the extent of the bend could not be intuitively predicted and the strain gauges give a valuable quantitative measure. It is this kind of information that is directly relevant to the modelling of such events.

The VISAR traces for the tungsten rods are all very similar showing a rounded, convex shape indicating a relatively slow acceleration over a period of ca. $20 \mu\text{s}$ to a velocity of $35\text{--}45 \text{ m s}^{-1}$. There is a break in the acceleration slope approximately $20 \mu\text{s}$ after the tail of the rod starts accelerating; this could be due to the effect of the rod tip striking the sabot carrying the plate. Pitch seems to have only a slight effect on the tail velocity of the rod: the rod at -9° pitch having a slightly faster acceleration. Their basic similarity, unlike the strain gauge traces, was probably due to the rods fragmenting, for a fragmented rod, while still having some penetration capability, would not transmit the stress pulse as effectively as an intact, though flexing rod. Examples of VISAR traces are shown in Fig. 33.

Due to the fragmentation of the tungsten rods, significant debris was generated at the impact point. The basic process for negative pitches was: initial contact with some bending, followed by some skidding along the impact face, bulging of the rear of the plate along the skid path and finally the rod pushing through. This process tended, however, to be obscured by a dense debris cloud. By contrast, for positively pitched rods, soon after they contact the surface, the rear of the

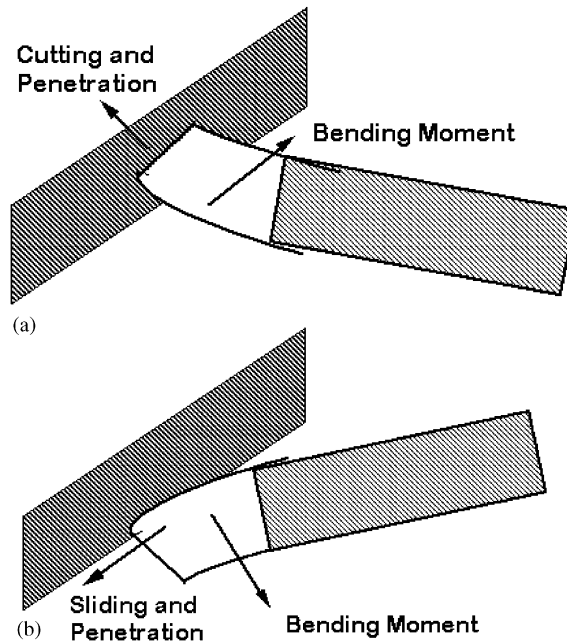


Fig. 32. Comparison of mechanisms for (a) positive and (b) negative pitches.

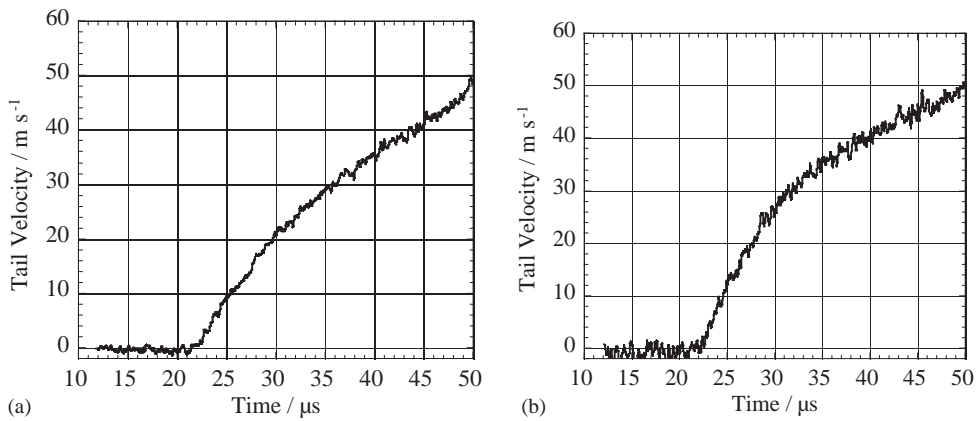


Fig. 33. Velocity histories of the rod tail with pitch (a) +6° and (b) -9°. From Ref. [282].

plate starts to bulge over a very small region, and the rod pushes through. The bulging of the rear of the plate occurs above the initial centre line of the rod indicating that the rod had bent into the plate surface as seen in Fig. 34.

Supporting evidence for these processes was found by comparing the hole shape and the length of any grooves around the hole cut into the surface on the impact surface: negative pitches had long grooves while positive pitches showed short steep cuts leading to the hole.

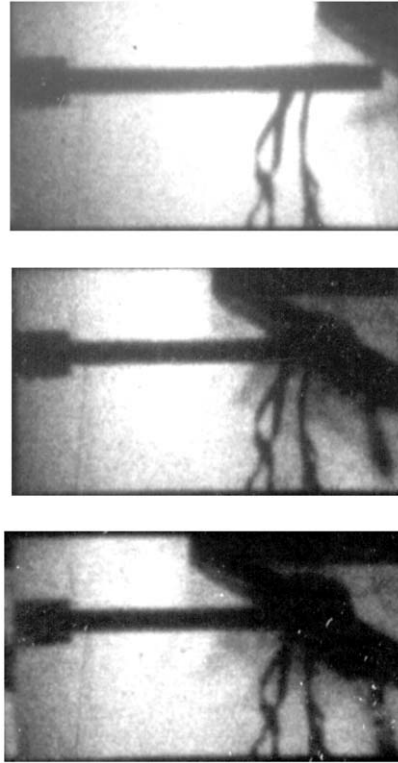


Fig. 34. Three frames from a high-speed sequence. Rod pitch $+3^\circ$ pitch, 200 ns exposure time, 4.8 μ s interframe time. From Ref. [282].

Ballistics represent a field in which data interpretation is difficult given the 3D nature of the problem and the mix of fracture and large plasticity effects generally seen. Progress will only be achieved by a combination of careful and extensive use of experimental diagnostics and computer modelling. To this end, the reverse ballistic geometry has proved to be invaluable in the generation of quantitative data.

7. Optical techniques for dynamic stress analysis

Conventional strain gauges measurements at a single point, combining a high degree of accuracy (a few microstrain) with good time resolution (usually of the order of tens of ns). However, strain gauges have two significant disadvantages: (i) they only give information at one point in the field of view and (ii) bonding the gauge to the specimen may provide local reinforcement which perturbs the stress field. Optical techniques, on the other hand, generally provide whole-field information and many are also non-contacting. A wide range of optical techniques have been developed for the measurement of displacement, strain and stress (see Table 3 and the references therein).

Many of the optical techniques currently used for studying dynamic events were originally developed for quasi-static applications. The *Handbook on Experimental Mechanics* [294,295]

Table 3
Summary of optical techniques for dynamic stress analysis

Method	The measurement	Sensitivity	Accuracy	Light source	References
Photoelasticity	$\sigma_1 - \sigma_2$	Variable	Variable	Incoherent	[294–297]
Caustics	$\partial u_z / \partial x, \partial u_z / \partial y$	Variable	Variable	Incoherent	[294,295,298–301]
Moiré	u_x or u_y	Grating pitch	$\sim p/10$	Coherent	[294,295,302,303]
interferometry		$p \approx \lambda$			
Moiré	u_x or u_y	Grating pitch	$\sim p/10$	Incoherent	[294,295,304]
photography		$p \approx 5\text{--}1000 \mu\text{m}$			
Speckle	u_x and u_y	Speckle diameter	$\sim 0.2\sigma^2 / (\text{spatial resolution})$	Coherent	[294,295,305,306]
photography		$\sigma \approx 5\text{--}50 \mu\text{m}$			
Digital speckle	u_x and u_y, u_z also possible	~ 1 pixel of digital image	$\sim 1/100$ pixel of digital image	Coherent or incoherent	[108,258,307–309]
photography					
Speckle	u_x, u_y or u_z	$\sim \lambda$	$\sim \lambda/10$	Coherent	[294,295,310]
interferometry					
Holographic	u_x, u_y and u_z	$\lambda/2$	$\sim \lambda/50$	Coherent	[294,295,311]
interferometry					
Shearing	$\partial u_x / \partial x$ or $\partial u_z / \partial y$	$\sim \lambda / (\text{shear distance})$	$\sim 0.1\lambda / (\text{shear distance})$	Coherent	[312]
interferometry					

provides an excellent background to the use of optical methods in experimental mechanics. In this section, we outline the most frequently used techniques, typical applications and some promising new methods. Table 3 provides a concise summary.

7.1. Photoelasticity

This is one of the oldest and most widely used photomechanics methods, and relies on the fact that some transparent materials become birefringent under an applied load. The birefringence is made visible by placing the sample between circular polarisers. A so-called isochromatic fringe pattern is formed, which in 2D represents contours of $\sigma_1 - \sigma_2$ where σ_1 and σ_2 are the principal in-plane stresses. The fringe sensitivity varies by several orders of magnitude between materials (e.g. $\sim 400 \text{ kN m}^{-1} \text{ fringe}^{-1}$ for glass to $0.2 \text{ kN m}^{-1} \text{ fringe}^{-1}$ for polyurethane rubber). Cranz-Schardin cameras are often used to record the fringe patterns due to their good spatial resolution. Photoelasticity is an appropriate technique for studying the response of model structures but is less useful for investigating the mechanical properties of opaque materials. It has been used extensively in dynamic fracture studies, e.g. Ref. [297] where the dynamic stress intensity factor, K_{Id} , can be estimated by least-squares fitting a series expansion of the theoretical stress field to the measured fringe pattern. Another example is visualisation of stress wave propagation through model granular materials [296]. There are, however, many other applications in the literature.

7.2. Caustics

This approach was proposed by Manogg [299] and used extensively by, for example, Theocaris and Gdoutos [300], Kalthoff [298], Zehnder and Rosakis [301] and their co-workers, mainly for

studies of dynamic fracture. A collimated beam of light illuminates the specimen surface and the reflected or transmitted beam is recorded by a camera focused on a plane separated from the specimen surface by a small distance. The intensity distribution depends on the surface slope distribution (and hence on the in-plane stresses), but the analysis of general stress fields is difficult. In the presence of a crack, however, the surface displacement of the specimen is inversely proportional to the square root of distance from the crack tip and the caustic pattern forms a characteristic, approximately circular, dark region centred on the crack tip. The diameter of this ‘shadow spot’ can be related directly to K_{I_d} . One of the main advantages of the technique is its experimental simplicity. If the crack is moving, it is even possible to multiply expose a single picture using a strobed light source, thereby avoiding the need for a high-speed camera.

7.3. Moiré

A family of moiré techniques has been developed to measure in-plane and out-of-plane displacement fields. For in-plane displacements, a grating is attached to the specimen surface. For large strains, images of the grating can be recorded directly onto film [313], but the usual approach when the strains are low is to form moiré fringes by superimposing a second reference grating of almost the same spatial frequency. The camera need then only resolve the fringe pattern and not the grating lines. The pattern represents a contour map of the in-plane displacement component perpendicular to the grating lines, with a contour interval or ‘sensitivity’ equal to the pitch p of the specimen grating. Specimen grating frequencies of up to about 40 lines per millimetre (sensitivity = 25 μm) can be used with white light illumination, but the sensitivity is dramatically improved (to sub-micron values) by the use of coherent light. The technique is then known as moiré interferometry. Applications include visualisation of stress waves in graphite epoxy composites [303] and dynamic fracture studies [302]. Intermediate sensitivities (5–10 μm) can be achieved by high-resolution moiré photography [304], first proposed by Burch and Forno [314], in which the specimen grating is imaged onto the reference grating with a masked camera lens. Fig. 35 shows a high-speed sequence of moiré fringe patterns produced in a PMMA plate following impact by a steel ball. The combination of an accuracy of $\sim 1\mu\text{m}$ together with microsecond time resolution make this method attractive for the dynamic stress analysis of many polymers and composites.

7.4. Laser speckle

A second family of techniques is based on the phenomenon of laser speckle, which is the granular pattern produced when a rough surface is illuminated by coherent light. The simplest method (termed ‘laser speckle photography’) involves recording double-exposure photographs of the object. The speckle pattern moves as though it were physically present on the specimen surface, so the displacement field occurring between the two exposures can be mapped out by measuring the speckle displacement point by point from the developed photograph. This is normally done by probing the photograph with a narrow laser beam and measuring the spacing and angle of the Young’s fringes in the diffraction halo. Fig. 36 shows a double-exposure photograph of a fast crack in PMMA recorded by a double-pulsed ruby laser with an

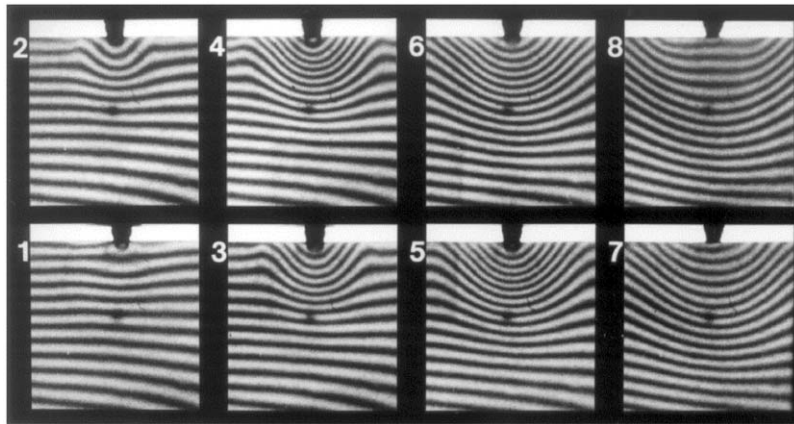


Fig. 35. High-resolution moiré fringe patterns showing displacement field produced by steel ball impact on PMMA (impact velocity $115 \pm 10 \text{ m s}^{-1}$). Horizontal grating, pitch = $6.7 \mu\text{m}$, interframe time = $0.95 \mu\text{s}$, field of view = $16 \times 16 \text{ mm}^2$. From Ref. [315].

open-shutter camera. The Young's fringes produced by probing the photograph at several points are also shown. Fig. 37 is the displacement field deduced by measuring 256 such fringe patterns.

The random error in the measured displacement component scales as the square of the diameter σ of the smallest speckle that can be resolved by the imaging system [305]. High-speed cameras with good spatial resolution are, therefore, necessary when recording sequences of speckle photographs. Crazz-Schardin cameras are unsuitable because light is scattered into all the lenses on each light pulse. Rotating mirror cameras with pulsed ruby laser light sources can, however, be used to measure displacement fields to sub-micron accuracy with fields of view of several tens of millimetres and a time resolution of order $1 \mu\text{s}$ [306]. The advantage of speckle photography over other techniques is that it is literally non-contacting and can be used on specimens with rough surfaces with little or no surface preparation required.

7.5. Speckle interferometry

This technique relies on the interference between two speckle patterns or a speckle pattern and smooth reference wave. Depending on the optical configuration, it can be used to measure in-plane or out-of-plane displacement fields. In the dynamic case, double-exposure photographs are recorded, and changes in speckle correlation due to the object displacement are made visible by spatial filtering. Fig. 38 is a sequence of fringe patterns from an in-plane speckle interferometer used to measure the transient displacement field round a stationary crack in an aluminium plate. The crack was loaded with a compressive stress pulse, and the exposures were recorded with a single-pulse ruby laser [310]. The sequence was built up by repeating the experiment several times with different time delays between the impact and laser pulse, but could have been recorded as one sequence using the camera/laser system described in Ref. [306]. The fringe pattern represents the same quantity (horizontal displacement component) with the same sensitivity ($0.4 \mu\text{m}$) as would be obtained with moiré interferometry, but no grating was required on the specimen surface.

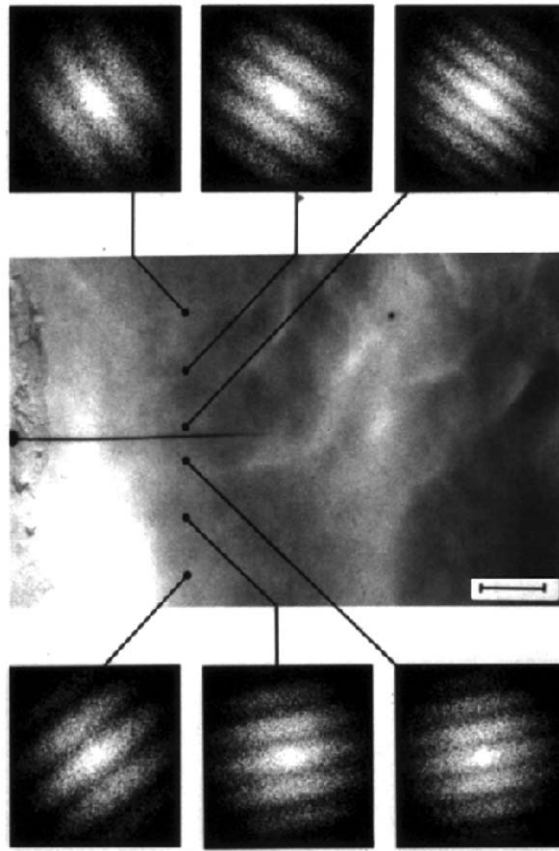


Fig. 36. Double-exposure speckle photograph of fast crack in PMMA. Time between exposures = $15 \mu\text{s}$; crack velocity $\approx 290 \text{ m s}^{-1}$. From Ref. [316].

7.6. Holographic interferometry

This is a related technique in which a double-exposure hologram is recorded of the object before and after deformation, using a double-pulsed ruby laser for example. When the hologram is reconstructed, a fringe pattern is observed which can be related to the displacement component along the bisector of the illumination and viewing directions. The technique produces very high-quality fringe patterns, requires no specimen preparation, and can be used whenever a ‘snapshot’ of the displacement field is required. Fallström et al. [311] describe one example of its application to the visualisation of waves in isotropic and anisotropic plates. It is difficult, however, to record sequences of holograms with a high-speed camera.

7.7. Shearing interferometry

This has been applied to dynamic fracture experiments under the name ‘coherent gradient sensor’ [312]. An interference pattern is formed between two copies of the image, one of which has

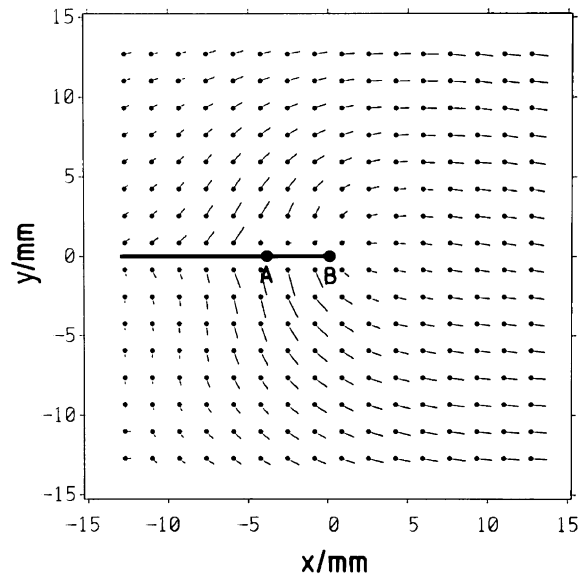


Fig. 37. Displacement field measured from Young’s fringe patterns, produced by pointwise filtering the photograph in Fig. 36. The crack has extended from A to B between exposures. From Ref. [316].

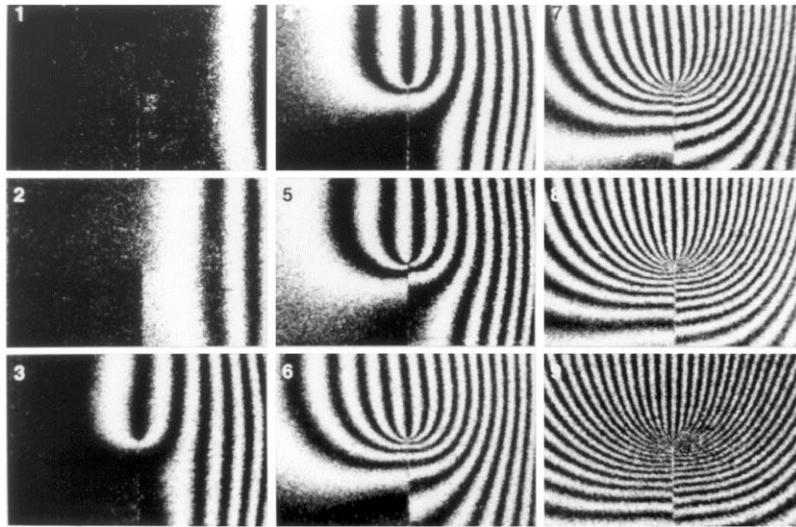


Fig. 38. Speckle interferometry fringe patterns showing the interaction of a stress wave with a vertical crack. Field of view $73 \times 49 \text{ mm}^2$. The times of each frame may be found in Ref. [310].

been laterally shifted or ‘sheared’ relative to the other. The fringes represent contours of constant surface gradient. The surface must have a mirror finish, but this has the advantage that the technique is much more efficient in its use of the available light than speckle or holographic

methods, so that much lower power lasers (e.g. cavity-dumped argon ion, rather than Q-switched ruby) can be used.

7.8. Digital speckle photography

Whilst in many ways fundamentally different from the double-exposure technique described above in Section 7.4, digital speckle photography can be regarded as its modern successor largely due to recent improvements in computing power and digital camera technology. If a specimen is illuminated as described above with coherent light to give a speckle pattern, ‘before’ and ‘after’ photographs are taken, then a digital cross-correlation algorithm is applied which compares small regions of each photograph and calculates the local displacement in that region [108,307–309]. By using a stereoscopic pair of cameras, it is possible to determine all three components of displacement simultaneously [258].

Of course, so long as the pattern being photographed on the specimen surface is random, it does not have to be produced directly by a laser. For example, Asay et al. [317] used a pattern of crystals caused to glow by laser-induced fluorescence as markers in an energetic composite being impacted by a flyer plate. Here, high-speed photography was also used to produce an entire sequence of results from a single experiment.

Extending the concept even further, it is possible to fabricate a sample to include a random pattern of dense particles on a plane within their bulk, and then take photographs with X-rays rather than optically. If X-ray flashes are used, the motion of dynamic systems can be studied effectively, since a typical X-ray flash will have a duration of as little as 30 ns. Thus, the internal deformations of various dynamic events can be studied [259–266,318]. Illustrated below in Fig. 39 is a polyester specimen $45 \times 45 \times 24 \text{ mm}^3$ cast with a plane of lead filings inside it [260]. This was impacted with a ball bearing travelling at 375 m s^{-1} . A stereoscopic pair of X-ray plates was exposed before the impact, and then another pair $20 \mu\text{s}$ after the impact. By scanning the developed films into a computer and applying a 3D digital speckle photography algorithm, the displacement map shown in Fig. 40 was calculated. This technique can even be applied to events as rapid as shaped charge jet impact [266] (Fig. 41).

The elegance and flexibility of the digital speckle photography technique have thus allowed it to spread into many areas of dynamic testing, since it can yield two or even three components of displacement, quasi-statically or dynamically, inside or on the surface of a specimen.

7.9. Dynamic infrared thermography

Recently, there has been renewed interest in the energy dissipated and temperature rises associated with bulk dynamic deformation and fracture, e.g. Refs. [319–325]. Infrared methods of measuring temperature are well established and have the advantages that they are non-invasive and can take measurements over a whole surface. However, care must be taken in interpreting the measurements made as the surface emissivity is often poorly known and may change during deformation. A fuller discussion of these problems may be found in Ref. [322]. The recent development of infrared high-speed framing photography on microsecond timescales [324] has opened up exciting possibilities for new discoveries, one such being the observation of hot spots in propagating adiabatic shear bands [323].

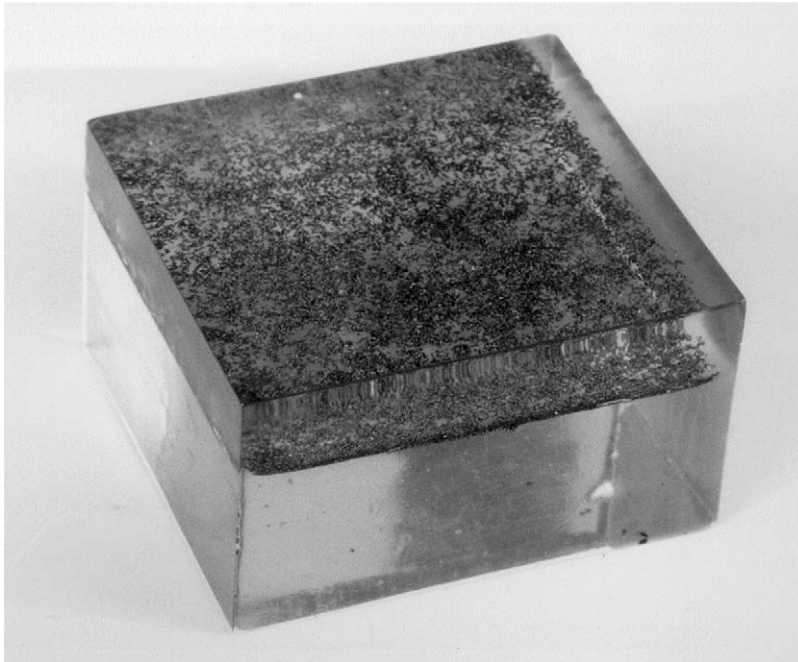


Fig. 39. Photograph of polyester specimen with lead filings scattered randomly on an internal plane.

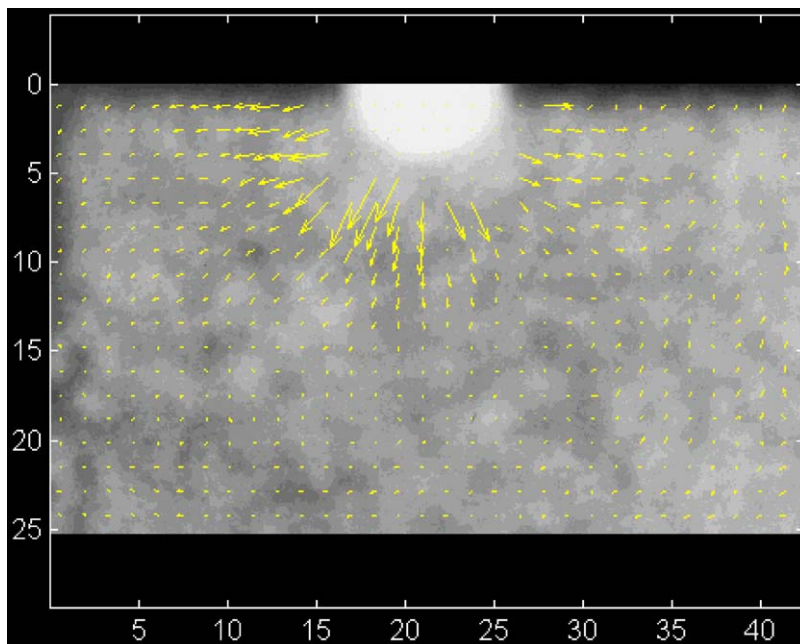


Fig. 40. Calculated in-plane displacement components superimposed on a radiograph taken $20 \mu\text{s}$ after the impact of a 9 mm ball bearing at 375 m s^{-1} on the specimen shown in Fig. 39. The arrows give the magnitude and direction of the displacements. From Ref. [260].

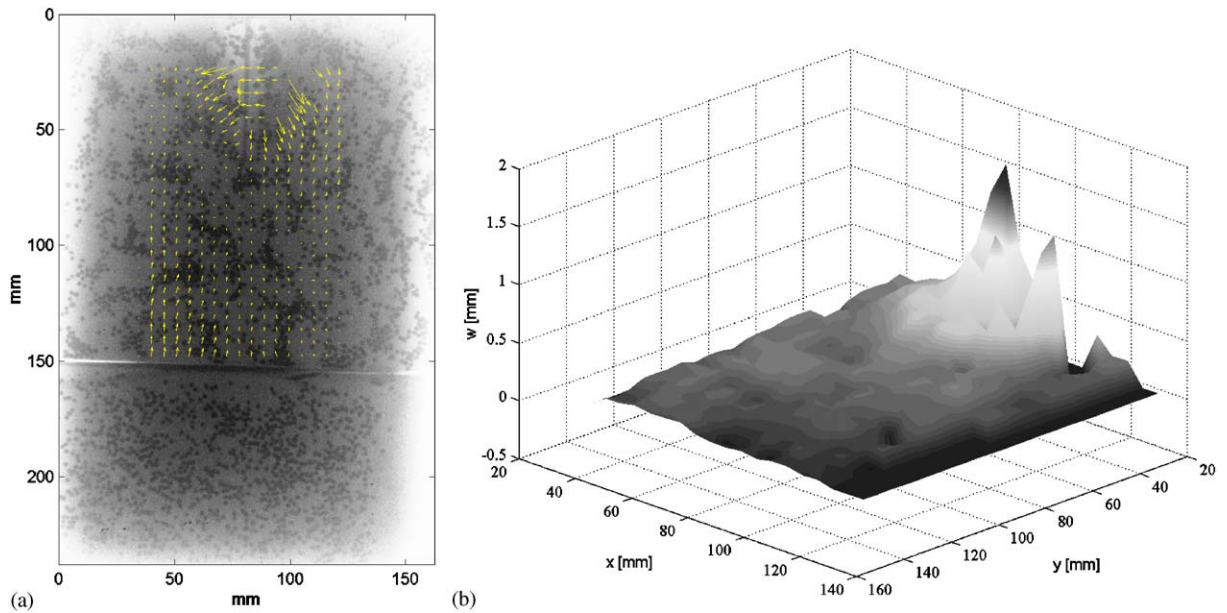


Fig. 41. Application of 3D Digital Speckle Radiography to 6 km s^{-1} shaped charge impact on concrete seeded with lead shot. (a) In-plane displacement components superimposed on a radiograph taken $18.5 \mu\text{s}$ after initiation of the shaped charge. (b) Out-of-plane displacements calculated using stereoscopic algorithm. From Ref. [266].

Acknowledgements

We thank Professors N.K. Bourne and J.M. Huntley for their input to earlier versions of this review. The Cambridge research in this area has been sponsored by EPSRC, MOD and the Royal Society. In particular, we thank Dr. A.D. Andrews, Dr. W.A. Carson, P.D. Church, Dr. I.G. Cullis, B. Goldthorpe, Dr. B. James, Dr. Y. Me-Bar, Dr. I.M. Pickup and Dr. Z. Rosenberg for their encouragement and advice.

References

- [1] Field JE, Walley SM, Bourne NK, Huntley JM. Experimental methods at high rates of strain. *J Phys IV France* 1994;4(C8):3–22.
- [2] Field JE, Walley SM, Bourne NK, Huntley JM. Review of experimental techniques for high rate deformation studies. In: *Proceedings of the Acoustics and Vibration Asia '98*. Singapore: Acoustics and Vibration Asia 98 Conference; 1998. p. 9–38.
- [3] Field JE, Proud WG, Walley SM, Goldrein HT. Review of experimental techniques for high rate deformation and shock studies. In: Nowacki WK, Klepaczko JR, editors. *New experimental methods in material dynamics and impact*. Warsaw, Poland: Institute of Fundamental Technological Research; 2001. p. 109–77.
- [4] Gorham DA. The effect of specimen dimensions on high strain rate compression measurements of copper. *J Phys D* 1991;24:1489–92.
- [5] Gorham DA, Pope PH, Field JE. An improved method for compressive stress–strain measurements at very high strain rates. *Proc R Soc Lond A* 1992;438:153–70.

- [6] Follansbee PS, Regazzoni G, Kocks UF. The transition to drag controlled deformation in copper at high strain rates. *Inst Phys Conf Ser* 1984;70:71–80.
- [7] Brace WF, Jones AH. Comparison of uniaxial deformation in shock and static loading of three rocks. *J Geophys Res* 1971;76:4913–21.
- [8] Armstrong RW. On size effects in polycrystal plasticity. *J Mech Phys Solids* 1961;9:196–9.
- [9] Armstrong RW. Plasticity: grain size effects. In: Buschow KHJ, Cahn RW, Flemings MC, Illschner B, Kramer EJ, Mahajan S, editors. *Encyclopedia of materials: science and technology*. Amsterdam: Elsevier; 2001. p. 7103–14.
- [10] Albertini C, Cadoni E, Labibes K. Study of the mechanical properties of plain concrete under dynamic loading. *Exp Mech* 1999;39:137–41.
- [11] Gorham DA. Measurement of stress–strain properties of strong metals at very high strain rates. *Inst Phys Conf Ser* 1980;47:16–24.
- [12] Bell JF. *The experimental foundations of solid mechanics*. Berlin: Springer; 1973.
- [13] Kuhn H, Medlin D, editors. *ASM handbook: mechanical testing and evaluation*, vol. 8. Materials Park, OH: ASM International; 2000.
- [14] Lichtenberger A, Gary G, Dodd B, Couque H, Kammerer C, Naulin G. *Test recommendation: dynamic compression testing using the split Hopkinson pressure bar*. Saint-Louis, France: DYMAT; 1999.
- [15] Couque H, Walley S, Lichtenberger A, Chartagnac P, Dormeval R, Petit J. *Test recommendation: dynamic compression testing using the Taylor test*. Arcueil, France: DYMAT; 2001.
- [16] Radford DD, Walley SM, Church P, Field JE. Dynamic upsetting and failure of metal cylinders: experiments and analysis. *J Phys IV France* 2003;110:263–8.
- [17] Pope PH. *Dynamic compression of metals and explosives*. PhD thesis, University of Cambridge, 1985.
- [18] Swallowe GM, Lee SF. A study of the mechanical properties of PMMA and PS at strain rates of 10^{-4} to 10^3 s $^{-1}$ over the temperature range 293–363 K. *J Phys IV France* 2003;110:33–8.
- [19] Mortlock HN, Wilby J. The Rotter apparatus for the determination of impact sensitiveness. *Explosivstoffe* 1966;14:49–55.
- [20] Heavens SN, Field JE. The ignition of a thin layer of explosive by impact. *Proc R Soc Lond A* 1974;338:77–93.
- [21] Field JE, Swallowe GM, Heavens SN. Ignition mechanisms of explosives during mechanical deformation. *Proc R Soc Lond A* 1982;382:231–44.
- [22] Field JE, Bourne NK, Palmer SJP, Walley SM. Hot-spot ignition mechanisms for explosives and propellants. *Philos Trans R Soc Lond A* 1992;339:269–83.
- [23] Walley SM, Field JE, Palmer SJP. Impact sensitivity of propellants. *Proc R Soc Lond A* 1992;438:571–83.
- [24] Walley SM, Balzer JE, Proud WG, Field JE. Response of thermites to dynamic high pressure and shear. *Proc R Soc Lond A* 2000;456:1483–503.
- [25] Walley SM, Field JE, Swallowe GM, Mentha SN. The response of various polymers to uniaxial compressive loading at very high rates of strain. *J Phys France* 1985;46(C5):607–16.
- [26] Hopkinson B. A method of measuring the pressure produced in the detonation of high explosives or by the impact of bullets. *Philos Trans R Soc Lond A* 1914;213:437–56.
- [27] Taylor GI. The testing of materials at high rates of loading. *J Inst Civ Eng* 1946;26:486–519.
- [28] Volterra E. Alcuni risultati di prove dinamiche sui materiali. *Riv Nuovo Cimento* 1948;4:1–28.
- [29] Kolsky H. An investigation of the mechanical properties of materials at very high rates of loading. *Proc Phys Soc Lond B* 1949;62:676–700.
- [30] Luerssen GV, Greene OV. The torsion impact test. *Proc Am Soc Testing Mater* 1933;33(2):315–33.
- [31] Mason W. The yield of steel wire under stresses of very small duration. *Proc Inst Mech Eng* 1934;128:409–38.
- [32] Mann HC. The relation between the tension static and dynamic tests. *Proc Am Soc Testing Mater* 1935;35(2):323–40.
- [33] Itihara M. Impact torsion test. *Technol Rep Tohoku Univ* 1935;11:16–50, 489–581; Itihara M. Impact torsion test. *Technol Rep Tohoku Univ* 1936;12:63–118.
- [34] Loizou N, Sims RB. The yield stress of pure lead in compression. *J Mech Phys Solids* 1953;1:234–43.
- [35] Harding J, Wood EO, Campbell JD. Tensile testing of materials at impact rates of strain. *J Mech Eng Sci* 1960;2:88–96.

- [36] Duffy J, Campbell JD, Hawley RH. On the use of a torsional split Hopkinson bar to study rate effects in 1100–0 aluminum. *Trans ASME: J Appl Mech* 1971;38:83–91.
- [37] Nemat-Nasser S. Recovery Hopkinson bar technique. In: Kuhn H, Medlin D, editors. *ASM handbook: mechanical testing and evaluation*, vol. 8. Materials Park, OH: ASM International; 2000. p. 477–87.
- [38] Gilat A. Torsional Kolsky bar testing. In: Kuhn H, Medlin D, editors. *ASM handbook: mechanical testing and evaluation*, vol. 8. Materials Park, OH: ASM International; 2000. p. 505–15.
- [39] Kocks UF, Stout MG. Torsion testing for general constitutive relations: Gilles Canova's masters thesis. *Model Simul Mater Sci Eng* 1999;7:675–81.
- [40] Gray III GT. Classic split-Hopkinson pressure bar testing. In: Kuhn H, Medlin D, editors. *ASM handbook: mechanical testing and evaluation*, vol. 8. Materials Park, OH: ASM International; 2000. p. 462–76.
- [41] Gray III GT. The split Hopkinson pressure bar: an evolving quantification tool and technique for constitutive model validation. Report No. LA-UR-01-5615, Los Alamos National Laboratory, 2001.
- [42] Meng H, Li QM. Correlation between the accuracy of a SHPB test and the stress uniformity based on numerical experiments. *Int J Impact Eng* 2003;28:537–55.
- [43] Zhao H. Material behaviour characterization using SHPB techniques, tests and simulations. *Comput Struct* 2003;81:1301–10.
- [44] Zhao H. Testing of polymeric foams at high and medium strain rates. *Polym Testing* 1997;16:507–16.
- [45] Yi F, Zhu ZG, Zu FQ, Hu SS, Yi P. Strain rate effects on the compressive property and the energy-absorbing capacity of aluminum alloy foams. *Mater Charact* 2001;47:417–22.
- [46] Hanssen AG, Enstock L, Langseth M. Close-range blast loading of aluminium foam panels. *Int J Impact Eng* 2002;27:593–618.
- [47] Lopatnikov SL, Gama BA, Haque MJ, Krauthauser C, Gillespie JW, Guden M, Hall IW. Dynamics of metal foam deformation during Taylor cylinder–Hopkinson bar impact experiment. *Compos Struct* 2003;61:61–71.
- [48] Gray III GT, Idar DJ, Blumenthal WR, Cady CM, Peterson PD. High- and low-strain rate compression properties of several energetic material composites as a function of strain rate and temperature. In: Short JM, Kennedy JE, editors. *Proceedings of the 11th International Detonation Symposium*. Arlington, VA: Office of Naval Research; 2000. p. 76–84.
- [49] Siviour CR, Walley SM, Proud WG, Field JE. Hopkinson bar studies on polymer bonded explosives. In: Vágenknecht J, editor. *Proceedings of the Sixth Seminar on New Trends in Research of Energetic Materials*. Pardubice, Czech Republic: University of Pardubice; 2003. p. 338–49.
- [50] Albertini C, Boone PM, Montagnini M. Development of the Hopkinson bar for testing large specimens in tension. *J Phys France* 1985;46(C5):499–504.
- [51] Nemat-Nasser S, Isaacs JB, Starrett JE. Hopkinson techniques for dynamic recovery experiments. *Proc R Soc Lond A* 1991;435:371–91.
- [52] Feng R, Ramesh KT. Dynamic behavior of elastohydrodynamic lubricants in shearing and compression. *J Phys IV France* 1991;1(C3):69–76.
- [53] Feng R, Ramesh KT. On the compressibility of elastohydrodynamic lubricants. *Trans ASME: J Tribol* 1993;115:557–9.
- [54] Feng R, Ramesh KT. The rheology of lubricants at high shear rates. *Trans ASME: J Tribol* 1993;115:640–9.
- [55] Wang LL, Labibes K, Azari Z, Pluvinage G. On the use of a viscoelastic bar in the split Hopkinson bar technique. In: Maekawa I, editor. *Proceedings of the International Symposium on Impact Engineering*. Sendai, Japan: ISIE; 1992. p. 532–7.
- [56] Wang L, Labibes K, Azari Z, Pluvinage G. Generalization of split Hopkinson bar technique to use viscoelastic bars. *Int J Impact Eng* 1994;15:669–86.
- [57] Gary G, Klepaczko JR, Zhao H. Generalization of split Hopkinson bar technique to use viscoelastic materials. *Int J Impact Eng* 1995;16:529–30.
- [58] Gary G, Rota L, Thomas JJ, Zhao H. Testing and modelling the dynamic behaviour of polymeric foams used in automotive industry dummies. In: Najjar J, editor. *Proceedings of the Ninth DYMAT Technical Conference: Material and Structural Modelling in Collision Research*. Arcueil, France: DYMAT, 1995. (Paper 2).
- [59] Wang L, Labibes K, Azari Z, Pluvinage G. Authors' reply to 'Generalization of split Hopkinson bar technique to use viscoelastic bars'. *Int J Impact Eng* 1995;16:530–1.

- [60] Gary G, Rota L, Zhao H. Testing viscous soft materials at medium and high strain rates. In: Kawata K, Shioiri J, editors. *Constitutive relation in high/very high strain rates*. Tokyo: Springer; 1996. p. 25–32.
- [61] Zhao H, Gary G. A three dimensional analytical solution of the longitudinal wave propagation in an infinite linear viscoelastic cylindrical bar: application to experimental techniques. *J Mech Phys Solids* 1995;43:1335–48.
- [62] Sawas O, Brar NS, Ramamurthy AC. High strain rate characterization of plastics using polymeric split Hopkinson bar. In: Schmidt SC, Tao WC, editors. *Shock compression of condensed matter 1995*. Woodbury, NY: American Institute of Physics; 1996. p. 581–4.
- [63] Rao S, Shim VPW, Quah SE. Dynamic mechanical properties of polyurethane elastomers using a nonmetallic Hopkinson bar. *J Appl Polym Sci* 1997;66:619–31.
- [64] Zhao H, Gary G, Klepaczko JR. On the use of a viscoelastic split Hopkinson pressure bar. *Int J Impact Eng* 1997; 19:319–30.
- [65] Bacon C. An experimental method for considering dispersion and attenuation in a viscoelastic Hopkinson bar. *Exp Mech* 1998;38:242–9.
- [66] Zhao H. A study of specimen thickness effects in the impact tests on polymers by numeric simulations. *Polymer* 1998;39:1103–6.
- [67] Yunoshev AS, Silvestrov VV. Development of the polymeric split Hopkinson bar technique. *J Appl Mech Tech Phys* 2001;42:558–64.
- [68] Zhao H, Gary G. On the behaviour characterisation of polymeric foams over a large range of strain rates. In: Chiba A, Tanimura S, Hokamoto K, editors. *Proceedings of the fourth International Symposium on Impact Engineering*. Amsterdam: Elsevier; 2001. p. 23–8.
- [69] Zhao H, Gary G. Behaviour characterization of polymeric foams over a large range of strain rates. *Int J Vehicle Des* 2002;30:135–45.
- [70] Benatar A, Rittel D, Yarin AL. Theoretical and experimental analysis of longitudinal wave propagation in cylindrical viscoelastic rods. *J Mech Phys Solids* 2003;51:1413–31.
- [71] Casem DT, Fourney W, Chang P. Wave separation in viscoelastic pressure bars using single-point measurements of strain and velocity. *Polym Testing* 2003;22:155–64.
- [72] Casem D, Fourney WL, Chang P. A polymeric SHPB instrumented with velocity gages. *Exp Mech* 2003;43: 420–7.
- [73] Zhao H, Gary G. A new method for the separation of waves: application to the SHPB technique for an unlimited duration of measurement. *J Mech Phys Solids* 1997;45:1185–202.
- [74] Bacon C. Separation of waves propagating in an elastic or viscoelastic Hopkinson pressure bar with three-dimensional effects. *Int J Impact Eng* 1999;22:55–69.
- [75] Othman R, Bussac MN, Collet P, Gary G. Increasing the maximum strain measured with elastic and viscoelastic Hopkinson bars. In: Chiba A, Tanimura S, Hokamoto K, editors. *Proceedings of the Fourth International Symposium on Impact Engineering*. Amsterdam: Elsevier; 2001. p. 49–56.
- [76] Othman R, Bussac M-N, Collet P, Gary G. Séparation et reconstruction des ondes dans les barres élastiques et viscoélastiques à partir de mesures redondantes. *CR Acad Sci Paris IIb* 2001;329:369–76.
- [77] Othman R, Blanc RH, Bussac M-N, Collet P, Gary G. Identification de la relation de dispersion dans les barres. *CR Mécanique* 2002;330:849–55.
- [78] Zhao PJ, Lok TS. A new method for separating longitudinal waves in a large diameter Hopkinson bar. *J Sound Vib* 2002;257:119–30.
- [79] Bussac M-N, Collet P, Gary G, Othman R. An optimisation method for separating and rebuilding one-dimensional dispersive waves from multi-point measurements: application to elastic or viscoelastic bars. *J Mech Phys Solids* 2002;50:321–49.
- [80] Gray III GT, Blumenthal WR. Split-Hopkinson pressure bar testing of soft materials. In: Kuhn H, Medlin D, editors. *ASM handbook: mechanical testing and evaluation*, vol. 8. Materials Park, OH: ASM International; 2000. p. 488–96.
- [81] Macdougall D. A radiant heating method for performing high-temperature high-strain-rate tests. *Meas Sci Technol* 1998;9:1657–62.
- [82] Lennon AM, Ramesh KT. A technique for measuring the dynamic behavior of materials at high temperatures. *Int J Plast* 1998;14:1279–92.

- [83] Bacon C, Hosten B, Bernard PA. Acoustic wave generation in viscoelastic rods by time-gated microwaves. *J Acoust Soc Am* 1999;106:195–201.
- [84] Bacon C, Brun A. Methodology for a Hopkinson bar test with a non-uniform viscoelastic bar. *Int J Impact Eng* 2000;24:219–30.
- [85] Bacon C, Lataillade JL. Development of the Kolsky–Hopkinson techniques and application for non-conventional testing. In: Nowacki WK, Klepaczko JR, editors. *New experimental methods in material dynamics and impact*. Warsaw, Poland: Institute of Fundamental Technological Research; 2001. p. 1–58.
- [86] Bacon C, Guilloriot E, Hosten B, Chimenti DE. Acoustic waves generated by pulsed microwaves in viscoelastic rods: modeling and experimental verification. *J Acoust Soc Am* 2001;110:1398–407.
- [87] Guilloriot E, Bacon C, Hosten B. Prediction of the generation of acoustic waves due to the penetration of pulsed microwaves in multilayer media. *J Acoust Soc Am* 2002;112:65–74.
- [88] Chichili DR, Ramesh KT. Recovery experiments for adiabatic shear localization: a novel experimental technique. *Trans ASME: J Appl Mech* 1999;66:10–20.
- [89] Othman R, Bussac MN, Collet P, Gary G. Testing with SHPB from quasistatic for dynamic strain rates. *J Phys IV France* 2003;110:397–404.
- [90] Grantham SG, Siviour CR, Proud WG, Walley SM, Field JE. Speckle measurements of sample deformation in the split Hopkinson pressure bar. *J Phys IV France* 2003;110:405–10.
- [91] Walley SM, Field JE. Strain rate sensitivity of polymers in compression from low to high strain rates. *DYMAT J* 1994;1:211–28.
- [92] Al-Maliky N, Fernandez JO, Parry DJ, Swallowe GM. Drops in the flow stress of semicrystalline polymers at very high rates of strain. *J Mater Sci Lett* 1998;17:1141–3.
- [93] McCrum NG, Read BE, Williams G. *Anelastic and dielectric effects in polymeric solids*. London: Wiley; 1967.
- [94] Balzer JE, Siviour CR, Walley SM, Proud WG, Field JE. Behaviour of ammonium perchlorate-based propellants and a polymer-bonded explosive under impact loading. *Proc R Soc Lond A* 2004;460:781–806.
- [95] Gilat A, Krishna K. The effects of strain rate and thickness on the response of thin layers of solder loaded in pure shear. *Trans ASME: J Electron Packaging* 1997;119:81–4.
- [96] Wang B, Yi S. Dynamic plastic behavior of 63 wt% Sn 37 wt% Pb eutectic solder under high strain rates. *J Mater Sci Lett* 2002;21:697–8.
- [97] Siviour CR, Williamson DM, Palmer SJP, Walley SM, Proud WG, Field JE. Dynamic properties of solders and solder joints. *J Phys IV France* 2003;110:477–82.
- [98] Cosculluela A, Cagnoux J, Collombet F. Uniaxial compression of alumina: structure, microstructure and strain rate. *J Phys IV France* 1991;1(C3):109–16.
- [99] Collombet F, Bacon C, Cosculluela A, Lataillade JL. Study of uniaxial dynamic compressive behaviour of alumina using split Hopkinson pressure bars. In: Aliabadi MH, Nisitani H, Cartwright DJ, editors. *Computational methods in fracture mechanics, vol. 2*. Barking, UK: Elsevier Applied Science; 1992. p. 419–38.
- [100] Lataillade J-L, Bacon C, Collombet F, Delaet M. The benefit of Hopkinson bar techniques for the investigation of composite and ceramic materials. In: Kinra VK, Clifton RJ, Johnson GC, editors. *Wave propagation and emerging technologies (AMD vol. 188)*. New York: American Society of Mechanical Engineers; 1994. p. 85–94.
- [101] Kanahashi H, Mukai T, Yamada Y, Shimojima K, Mabuchi M, Aizawa T, Higashi K. Experimental study for the improvement of crashworthiness in AZ91 magnesium foam controlling its microstructure. *Mater Sci Eng A* 2001;308:283–7.
- [102] Deshpande VS, Fleck NA. High strain rate compressive behaviour of aluminium alloy foams. *Int J Impact Eng* 2000;24:277–98.
- [103] Reid SR, Tan PJ, Harrigan JJ. The crushing strength of aluminium alloy foam at high rates of strain. In: Chiba A, Tanimura S, Hokamoto K, editors. *Impact engineering and application*. Amsterdam: Elsevier; 2001. p. 15–22.
- [104] Abdennadher A, Zhao H, Othman R. A study of cellular materials under impact loading. *J Phys IV France* 2003;110:441–6.
- [105] Abdennadher S, Zhao H. A study of inertia effects under impact loading. *Key Eng Mater* 2003;233:223–8.
- [106] Bell JF. An experimental diffraction grating study of the quasi-static hypothesis of the SHPB experiment. *J Mech Phys Solids* 1966;14:309–27.
- [107] Chiang FP, Asundi A. White light speckle method of experimental strain analysis. *Appl Opt* 1979;18:409–11.

- [108] Sjö Dahl M, Benckert LR. Electronic speckle photography: analysis of an algorithm giving the displacement with subpixel accuracy. *Appl Opt* 1993;32:2278–84.
- [109] Chiang FP. A family of 2D and 3D experimental stress analysis techniques using laser speckle. *Solid Mech Arch* 1978;3:1–32.
- [110] Asundi A, Chiang FP. Measurement of large deformations using the white light speckle method. *Mech Res Commun* 1982;9:325–30.
- [111] Huntley JM, Whitworth MB, Palmer SJP, Goldrein HT, Field JE. Automatic speckle photography fringe analysis: application to electron microscopy and high speed photography. In: *Proceedings of the International Conference Hologram Interferometry and Speckle Metrology*. Bethel, CT: Society for Experimental Mechanics; 1990. p. 337–42.
- [112] Rae PJ, Palmer SJP, Goldrein HT, Lewis AL, Field JE. White-light digital image cross-correlation (DICC) analysis of the deformation of composite materials with random microstructure. *Opt Lasers Eng* 2004;41:635–48.
- [113] Grantham SG, Siviour CR, Proud WG, Field JE. High strain rate Brazilian testing using speckle metrology. *Meas Sci Technol* 2004, submitted for publication.
- [114] Taylor GI. The use of flat ended projectiles for determining yield stress. I: theoretical considerations. *Proc R Soc Lond A* 1948;194:289–99.
- [115] Whiffin AC. The use of flat ended projectiles for determining yield stress. II: tests on various metallic materials. *Proc R Soc Lond A* 1948;194:300–22.
- [116] Carrington WE, Gayler MLV. The use of flat ended projectiles for determining yield stress. III: changes in microstructure caused by deformation at high striking velocities. *Proc R Soc Lond A* 1948;194:323–31.
- [117] Bell JF. An experimental study of instability phenomena in the initiation of plastic waves in long rods. In: Lindholm US, editor. *Mechanical behavior of materials under dynamic loads*. Berlin: Springer; 1968. p. 10–20.
- [118] Erlich DC. Rod impact (Taylor) test. In: *Metals handbook*, 9th ed., vol. 8. Metals Park, OH: American Society of Metals; 1985. p. 203–7.
- [119] Maudlin PJ, Gray III GT, Cady CM, Kaschner GC. High-rate material modelling and validation using the Taylor cylinder impact test. *Philos Trans R Soc Lond A* 1999;357:1707–29.
- [120] Walley SM, Church PD, Townsley R, Field JE. Validation of a path-dependent constitutive model for FCC and BCC metals using ‘symmetric’ Taylor impact. *J Phys IV France* 2000;10(Pr. 9):69–74.
- [121] Murray NH, Bourne NK, Field JE, Rosenberg Z. Symmetrical Taylor impact of glass bars. In: Schmidt SC, Dandekar DP, Forbes JW, editors. *Shock compression of condensed matter—1997*. Woodbury, NY: American Institute of Physics; 1998. p. 533–6.
- [122] Radford DD, Willmott GR, Walley SM, Field JE. Failure mechanisms in ductile and brittle materials during Taylor impact. *J Phys IV France* 2003;110:687–92.
- [123] Hutchings IM. Estimation of yield stress in polymers at high strain rates using G.I. Taylor’s impact technique. *J Mech Phys Solids* 1978;26:289–301.
- [124] Church PD, Andrews T, Goldthorpe B. A review of constitutive model development within DERA. In: Jerome DM, editor. *Structures under extreme loading conditions*. PVP, vol. 394. New York: American Society of Mechanical Engineers; 1999. p. 113–20.
- [125] Forde LC. Ballistic impact of rods. PhD thesis, University of Cambridge, 2000.
- [126] McQueen RG, Marsh SP. Equation of state for nineteen metallic elements from shock-wave measurements to two megabars. *J Appl Phys* 1960;31:1253–69.
- [127] Prat C, Autric M. High power laser radiation induced shock waves in solids. In: Brun R, Dumitrescu LZ, editors. *Shock waves @ Marseille III*. Berlin: Springer; 1995. p. 255–60.
- [128] Trunin RF. *Shock compression of condensed materials*. Cambridge: Cambridge University Press; 1998.
- [129] Kanel GI, Asay JR, Baumung K, Bluhm H, Chhabildas LC, Fortov VE, Goel B, Hoppé P, Mehlhorn T, Razorenov SV, Rusch D, Utkin AV. Applications of the ion beam technique for investigations of hypervelocity impacts. *Int J Impact Eng* 1999;23:421–30.
- [130] Gray III GT. Shock wave testing of ductile materials. In: Kuhn H, Medlin D, editors. *ASM handbook: mechanical testing and evaluation*, vol. 8. Materials Park, OH: ASM International; 2000. p. 530–8.
- [131] Altshuler LV. Phase transitions in shock waves: a review. *J Appl Mech Tech Phys* 1978;19:496–505.
- [132] Davison L, Graham RA. Shock compression of solids. *Phys Rep* 1979;55:255–379.

- [133] Asay JR, Shahinpoor M, editors. High-pressure shock compression of solids. New York: Springer; 1993.
- [134] Fosdick R, Dunn E, Slemrod M, editors. Shock induced transitions and phase structures in general media. Berlin: Springer; 1993.
- [135] Graham RA. Solids under high-pressure shock compression. Berlin: Springer; 1993.
- [136] Sawaoka AB, editor. Shock waves in materials science. Berlin: Springer; 1993.
- [137] Batsanov AS. Effects of explosions on materials. New York: Springer; 1994.
- [138] Gathers GR. Selected topics in shock wave physics and equation of state modeling. Singapore: World Scientific; 1994.
- [139] Meyers MA. Dynamic behavior of materials. New York: Wiley Interscience; 1994.
- [140] Trunin RF. Shock compressibility of condensed materials in strong shock waves generated by underground nuclear explosions. *Phys Uspekhi* 1994;37:1123–45.
- [141] Cooper PW. Explosives engineering. New York: Wiley; 1996.
- [142] Davison L, Grady DE, Shahinpoor M, editors. High-pressure shock compression of solids II: dynamic fracture and fragmentation. New York: Springer; 1996.
- [143] Davison L, Horie Y, Shahinpoor M, editors. High-pressure shock compression of solids IV: response of highly porous solids to shock compression. New York: Springer; 1997.
- [144] Trunin RF. Comparison of the laboratory data on the compressibility of materials with the results obtained during underground nuclear explosions. *High Temp* 1997;35:888–95.
- [145] Davison L, Shahinpoor M, editors. High-pressure shock compression of solids III. New York: Springer; 1998.
- [146] Johnson JN, Chéret R, editors. Classic papers in shock compression science. New York: Springer; 1998.
- [147] Altshuler LV, Trunin RF, Urlin VD, Fortov VE, Funtikov AI. Development of dynamic high-pressure techniques in Russia. *Phys Uspekhi* 1999;42:261–80.
- [148] Dremin AN. Toward detonation theory. Berlin: Springer; 1999.
- [149] Wilkins ML. Computer simulation of dynamic phenomena. Berlin: Springer; 1999.
- [150] Nesterenko VF. Dynamics of heterogeneous materials. Berlin: Springer; 2001.
- [151] Ben-Dor G, Igra O, Elperin T, editors. Handbook of shock waves: Theoretical, experimental, and numerical techniques, vol. 1. New York: Academic Press; 2001.
- [152] Ben-Dor G, Igra O, Elperin T, editors. Handbook of shock waves: shock wave interactions and propagation, vol. 2. New York: Academic Press; 2001.
- [153] Ben-Dor G, Igra O, Elperin T, Lifshitz A, editors. Handbook of shock waves: chemical reactions in shock waves and detonations, vol. 3. New York: Academic Press; 2001.
- [154] Munson DE, May RP. Interior ballistics of a two-stage light gas gun using velocity interferometry. *AIAA J* 1976;14:235–42.
- [155] Kondo K, Hironaka Y, Ito H, Sugiura H, Ozaki S, Takeba A, Katayama M. A trial of the three-stage light gas gun with a preheating stage. In: Schmidt SC, Tao WC, editors. Shock compression of condensed matter 1995. Woodbury, NY: American Institute of Physics; 1996. p. 1193–6.
- [156] Marsh SP. LASL shock Hugoniot data. Berkeley, CA: University of California Press; 1980.
- [157] Grady DE. The spall strength of condensed matter. *J Mech Phys Solids* 1988;36:353–84.
- [158] Dunn JE, Fosdick R, Slemrod M, editors. Shock induced transitions and phase structures in general media. Berlin: Springer; 1993.
- [159] Sekine T. Shock wave chemical synthesis. *Eur J Solid State Inorg Chem* 1997;34:823–33.
- [160] Willmott GR, Proud WG, Field JE. Shock properties of diamond and kimberlite. *J Phys IV France* 2003;110:833–8.
- [161] Frey JD, Janicot F, Garaud X, Groenenboom P, Lambert M. The validation of hydrocodes for orbital debris impact simulation. *Int J Impact Eng* 1993;14:255–65.
- [162] Yoo CS, Holmes NC, Ross M, Webb DJ, Pike C. Shock temperatures and melting of iron at Earth core conditions. *Phys Rev Lett* 1993;70:3931–4.
- [163] Crossland B. Explosive welding of metals and its application. Oxford: Clarendon Press; 1982.
- [164] Rosenberg Z, Yaziv D, Partom Y. Calibration of foil-like manganin gauges in planar shock wave experiments. *J Appl Phys* 1980;51:3702–5.

- [165] Rosenberg Z. Determination of dynamic release curves of manganin stress gauges from their resistive hysteresis. *J Appl Phys* 1986;60:3369–71.
- [166] Grady DE, Ginsberg MJ. Piezoresistive effects in ytterbium stress transducers. *J Appl Phys* 1977;48:2179–81.
- [167] Brar NS, Gupta YM. Piezoresistance response of ytterbium foil gauges shocked to 45 kbar in fused silica matrix. *J Appl Phys* 1987;61:1304–10.
- [168] Stankiewicz J, White RL. Carbon resistors as pressure gauges. *Rev Sci Instrum* 1971;42:1067.
- [169] Ginsberg MJ, Asay BW. Commercial carbon composition resistors as dynamic stress gauges in difficult environments. *Rev Sci Instrum* 1991;62:2218–27.
- [170] Austing JL, Tulis AJ, Hrdina DJ, Baker DE, Martinez R. Carbon resistor gauges for measuring shock and detonation pressures. 1: principles of functioning and calibration. *Propell Explos Pyrotech* 1991;16:205–15.
- [171] Stanton PL, Graham RA. Shock wave compression of lithium niobate from 2.4 to 44 GPa. *J Appl Phys* 1979;50:6892–901.
- [172] Kenner VH. On the use of quartz crystals in dynamic stress and force transducers. *Exp Mech* 1975;15:102–6.
- [173] Close JA, Stevens R. The transient piezoelectric response of impact loaded PZT ceramics. *Ferroelectrics* 1992;134:181–7.
- [174] Sirohi J, Chopra I. Fundamental understanding of piezoelectric strain sensors. *J Intelligent Mater System Struct* 2000;11:246–57.
- [175] Bauer F, Graham RA. Behaviour of VF_2/VF_3 piezoelectric copolymers under shock loading. In: Schmidt SC, Johnson JN, Davidson LW, editors. *Shock compression of condensed matter—1989*. Amsterdam: Elsevier; 1990. p. 793–6.
- [176] Bauer F. PVDF shock sensors: applications to polar materials and high explosives. *IEEE Trans Ultrason Ferroelect Freq Control* 2000;47:1448–54.
- [177] Obara T, Bourne NK, Mebar Y. The construction and calibration of an inexpensive PVDF stress gauge for fast pressure measurements. *Meas Sci Technol* 1995;6:345–8.
- [178] Barker LM, Hollenbach RE. Laser interferometer for measuring high velocities of any reflecting surface. *J Appl Phys* 1972;43:4669–75.
- [179] Abou-Sayed AS, Clifton RJ, Hermann L. The oblique-plate impact experiment. *Exp Mech* 1976;16:127–32.
- [180] Mashimo T, Ozaki S, Nagayama K. Keyed powder gun for the oblique impact shock study of solids in several 10s of GPa region. *Rev Sci Instrum* 1984;55:226–30.
- [181] Meyer LW, Behler FJ, Frank K, Magness LS. Interdependencies between the dynamic mechanical properties and the ballistic behavior of materials. In: *Proceedings of the 12th International Symposium on Ballistics*, vol. 1. Arlington, VA: American Defence Preparedness Association; 1990. p. 419–28.
- [182] Rosenberg Z, Partom Y. Lateral stress measurement in shock-loaded targets with transverse piezoresistance gauges. *J Appl Phys* 1985;58:3072–6.
- [183] Rosenberg Z, Brar NS. The influence of the elasto-plastic properties of piezoresistive gauges on their loading-unloading characteristics as lateral shock stress transducers. *J Appl Phys* 1995;77:1443–8.
- [184] Bourne NK, Rosenberg Z, Millett JCF. The plate impact response of three glasses. In: Jones N, Brebbia CA, Watson AJ, editors. *Structures under shock and impact IV*. Southampton: Computational Mechanics Publications; 1996. p. 553–62.
- [185] Yaziv D, Bless SJ, Rosenberg Z. Study of spall and recompaction of ceramics using a double-impact technique. *J Appl Phys* 1985;58:3415–8.
- [186] Lopatin CM, Bless SJ, Brar NS. Dynamic unloading behavior of soda lime glass. *J Appl Phys* 1989;66:593–5.
- [187] Raiser G, Clifton RJ, Ortiz M. A soft-recovery plate impact experiment for studying microcracking in ceramics. *Mech Mater* 1990;10:43–58.
- [188] Gran JK, Seaman L. Analysis of piezoresistive gauges for stress in divergent flow fields. *ASCE: J Eng Mech* 1997;123:36–44.
- [189] Longy F, Cagnoux J. Macro- and micro-mechanical aspects of shock-loading of aluminas. In: Chiem CY, Kunze H-D, Meyer LW, editors. *Impact loading and dynamic behaviour of materials*. Oberursel, Germany: DGM Informationsgesellschaft mbH; 1988. p. 1001–8.
- [190] Rosenberg Z, Yeshurun Y. The relation between ballistic efficiency and compressive strength of ceramic tiles. *Int J Impact Eng* 1988;7:357–62.

- [191] Rosenberg Z, Brar NS, Bless SJ. Determination of the strength of shock loaded ceramics using double impact techniques. In: Schmidt SC, Johnson JN, Davidson LW, editors. Shock compression of condensed matter—1989. Amsterdam: Elsevier; 1990. p. 385–8.
- [192] Yeshurun Y, Rosenberg G, Rosenberg Z. Measurements of compressive and tensile waves in a shock loaded pyrex glass. In: Gupta YM, editor. Shock waves in condensed matter. New York: Plenum Press; 1986. p. 431–5.
- [193] Bless SJ, Brar NS, Rosenberg Z. Strength of soda lime glass under shock compression. In: Schmidt SC, Holmes NC, editors. Shock waves in condensed matter 1987. Amsterdam: North-Holland; 1988. p. 309–12.
- [194] Rosenberg Z, Marmor E, Maysel M. On the hydrodynamic theory of long-rod penetration. *Int J Impact Eng* 1990;10:483–6.
- [195] Kanel GI, Molodets AM, Dremin AN. Investigation of singularities of glass strain under intense compression waves. *Combust Explos Shock Waves* 1977;13:772–7.
- [196] Rasorenov SV, Kanel GI, Fortov VE, Abasehov MM. The fracture of glass under high pressure impulsive loading. *High Press Res* 1991;6:225–32.
- [197] Bourne NK, Rosenberg Z, Field JE. High-speed photography of compressive failure waves in glasses. *J Appl Phys* 1995;78:3736–9.
- [198] Bourne NK, Rosenberg Z. The dynamic response of soda-lime glass. In: Schmidt SC, Tao WC, editors. Shock compression of condensed matter 1995. Woodbury, NY: American Institute of Physics; 1996. p. 567–72.
- [199] Bourne NK, Millett JCF, Rosenberg Z. On the origin of failure waves in glass. *J Appl Phys* 1997;81:6670–4.
- [200] Brar NS. Failure waves in glass and ceramics under shock compression. In: Furnish MD, Chhabildas LC, Hixson RS, editors. Shock Compression of condensed matter—1999. Melville, NY: American Institute of Physics; 2000. p. 601–6.
- [201] Orphal DL, Kozhushko AA, Sinani AB. Possible detection of failure wave velocity in SiC using hypervelocity penetration experiments. In: Furnish MD, Chhabildas LC, Hixson RS, editors. Shock compression of condensed matter—1999. Melville, NY: American Institute of Physics; 2000. p. 577–80.
- [202] Staehler JM, Predebon WW, Pletka BJ. The response of a high purity alumina to plate impact testing. In: Schmidt SC, Shaner JW, Samara GA, Ross M, editors. High pressure science and technology 1993. New York: American Institute of Physics; 1994. p. 745–8.
- [203] Murray NH, Millett JCF, Proud WG, Rosenberg Z. Issues surrounding lateral stress measurements in alumina ceramics. In: Furnish MD, Chhabildas LC, Hixson RS, editors. Shock compression of condensed matter—1999. Melville, NY: American Institute of Physics; 2000. p. 581–4.
- [204] Murray NH, Proud WG. Measurement of lateral stress and spall strength in ceramics. In: Staudhammer KP, Murr LE, Meyers MA, editors. Fundamental issues and applications of shock-wave and high-strain-rate phenomena. New York: Elsevier; 2001. p. 151–6.
- [205] Grady DE. Shock wave compression of brittle solids. *Mech Mater* 1998;29:181–203.
- [206] Marom H, Sherman D, Rosenberg Z. Decay of elastic waves in alumina. *J Appl Phys* 2000;88:5666–70.
- [207] Kozhushko AA, Orphal DL, Sinani AB, Franzen RR. Possible detection of failure wave velocity using hypervelocity penetration experiments. *Int J Impact Eng* 1999;23:467–76.
- [208] Satapathy S, Bless S, Ivanov SM. The effects of failure wave on penetration resistance of glass. In: Reinecke WG, editor. Proceedings of the 18th International Symposium on Ballistics. Lancaster, PA: Technomic Publishing Company, Inc.; 1999. p. 1159–67.
- [209] Zilberbrand EL, Vlasov AS, Cazamias JU, Bless SJ, Kozhushko AA. Failure wave effects in hypervelocity penetration. *Int J Impact Eng* 1999;23:995–1002.
- [210] Mott NF. Fragmentation of shell cases. *Proc R Soc Lond A* 1947;189:300–8.
- [211] Mott NF. Fracture of metals: theoretical considerations. *Engineering* 1948;165:16–8.
- [212] Grady DE, Kipp ME. The micromechanics of impact fracture of rock. *Int J Rock Mech Min Sci* 1979;16:293–302.
- [213] Grady DE. Fragmentation of solids under impulsive stress loading. *J Geophys Res* 1981;86:1047–54.
- [214] Grady DE, Kipp ME. Geometric statistics and dynamic fragmentation. *J Appl Phys* 1985;58:1210–22.
- [215] Grady DE, Wilson LT, Reedal DR, Kuhns LD, Kipp ME, Black JW. Comparing alternate approaches in the scaling of naturally fragmenting munitions. In: Crewther IR, editor. Proceedings of the 19th International Symposium on Ballistics, Interlaken, Switzerland, 2001. p. 591–7.

- [216] Grady DE, Olsen ML. A statistics and energy based theory of dynamic fragmentation. *Int J Impact Eng* 2003;29:293–306.
- [217] Kipp ME, Grady DE, Chen EP. Strain-rate dependent fracture initiation. *Int J Fract* 1980;16:471–8.
- [218] Kipp ME, Grady DE. Dynamic fracture growth and interaction in one dimension. *J Mech Phys Solids* 1985;33:399–415.
- [219] Johnson GR, Holmquist TJ. A computational constitutive model for brittle materials subjected to large strains, high strain rates and high pressures. In: Meyers MA, Murr LE, Staudhammer KP, editors. *Shock-wave and high-strain-rate phenomena in materials*. New York: Marcel-Dekker; 1992. p. 1075–82.
- [220] Johnson GR, Holmquist TJ. An improved computational constitutive model for brittle materials. In: Schmidt SC, Shaner JW, Samara GA, Ross M, editors. *High pressure science and technology 1993*. New York: American Institute of Physics; 1994. p. 981–4.
- [221] Holmquist TJ, Johnson GR. Determination of constants and comparison of results for various constitutive models. *J Phys IV France* 1991;1(C3):853–60.
- [222] Clifton RJ. Analysis of failure waves in glasses. *Appl Mech Rev* 1993;46:540–6.
- [223] Steinberg DJ, Tipton RE. A new fracture model for ceramics. *Chem Phys Rep* 1995;14:321–7.
- [224] Rosenberg Z, Brar NS, Bless SJ. Elastic precursor decay in ceramics as determined with manganin strain gauges. *J Phys France Colloq* 1988;49(C3):707–12.
- [225] Yaziv D, Yeshurun Y, Partom Y, Rosenberg Z. Shock structure and precursor delay in commercial alumina. In: Schmidt SC, Holmes NC, editors. *Shock waves in condensed matter 1987*. Amsterdam: North-Holland; 1988. p. 297–300.
- [226] Murray NH, Bourne NK, Rosenberg Z. Precursor decay in several aluminas. In: Schmidt SC, Tao WC, editors. *Shock compression of condensed matter 1995*. Woodbury, NY: American Institute of Physics; 1996. p. 491–4.
- [227] Murray NH, Bourne NK, Rosenberg Z. The dynamic compressive strength of aluminas. *J Appl Phys* 1998; 84:4866–71.
- [228] Grady DE, Hollenbach RE, Schuler KW, Callender JF. Strain rate dependence in Dolomite inferred from impact and static compression tests. *J Geophys Res* 1977;82:1325–33.
- [229] Grady DE. Shock-wave properties of brittle solids. In: Schmidt SC, Tao WC, editors. *Shock compression of condensed matter 1995*. Woodbury, NY: American Institute of Physics; 1996. p. 9–20.
- [230] Bourne NK, Millett JCF, Rosenberg Z, Murray NH. On the shock induced failure of brittle solids. *J Mech Phys Solids* 1998;46:1887–908.
- [231] Bourne NK, Millett JCF, Field JE. On the strength of shocked glasses. *Proc R Soc Lond A* 1999;455: 1275–82.
- [232] Radford DD, Proud WG, Field JE. The deviatoric response of three dense glasses under shock loading conditions. In: Furnish MD, Thadhani NN, Horie Y, editors. *Shock compression of condensed matter—2001*. Melville, NY: American Institute of Physics; 2002. p. 807–10.
- [233] Brar NS, Espinosa HD. A review of micromechanics of failure waves in silicate glasses. *Chem Phys Rep* 1998;17:317–42.
- [234] Abeyaratne R, Knowles JK. A phenomenological model for failure waves in glass. *Shock Waves* 2000;10: 301–5.
- [235] Plekhov OA, Eremeev DN, Naimark OB. Failure wave as resonance excitation of collective burst modes of defects in shocked brittle materials. *J Phys IV France* 2000;10(Pr. 9):811–6.
- [236] Tate A. A theory for the deceleration of long rods after impact. *J Mech Phys Solids* 1967;15:387–99.
- [237] Tate A. Further results in the theory of long rod penetration. *J Mech Phys Solids* 1969;17:141–50.
- [238] Sternberg J. Material properties determining the resistance of ceramics to high velocity penetration. *J Appl Phys* 1989;65:3417–24.
- [239] Rosenberg Z, Tsaliah J. Applying Tate's model for the interaction of long rod projectiles with ceramic targets. *Int J Impact Eng* 1990;9:247–51.
- [240] Bless SJ, Rosenberg Z, Yoon B. Hypervelocity penetration of ceramics. *Int J Impact Eng* 1987;5:165–72.
- [241] Rosenberg Z, Yeshurun Y, Bless SJ, Okajima K. A new definition of ballistic efficiency of brittle materials based on the use of thick backing plates. In: Chiem CY, Kunze H-D, Meyer LW, editors. *Impact loading and dynamic behaviour of materials*. Oberursel, Germany: DGM Informationsgesellschaft mbH; 1988. p. 491–8.

- [242] Rosenberg Z, Yeshurun Y. An empirical relation between the ballistic efficiency of ceramic tiles and their effective compressive strength. In: Proceedings of the 11th Ballistics Conference. Brussels: Royal Military Academy; 1989. p. 501–6.
- [243] Forrestal MJ, Longcope DB. Target strength of ceramic materials for high-velocity penetration. *J Appl Phys* 1990;67:3669–72.
- [244] Shockey DA, Marchand AH, Skaggs SR, Cort GE, Burkett MW, Parker R. Failure phenomenology of confined ceramic targets and impacting rods. *Int J Impact Eng* 1990;9:263–75.
- [245] Curran DR, Seaman L, Cooper T, Shockey DA. Micromechanical model for comminution and granular flow of brittle material under high strain rate application to penetration of ceramic targets. *Int J Impact Eng* 1993;13:53–84.
- [246] Chen EP. Penetration into dry porous rock: a numerical study on sliding friction simulation. *Theor Appl Fract Mech* 1989;11:241–7.
- [247] Rule WK, Jones SE. Some remarks on the optimal nose geometry of a rigid penetrator in the presence of friction. In: Jerome DM, editor. Structures under extreme loading conditions. PVP, vol. 394. New York: American Society of Mechanical Engineers; 1999. p. 11–7.
- [248] Jones SE, Rule WK. On the optimal nose geometry for a rigid penetrator, including the effects of pressure-dependent friction. *Int J Impact Eng* 2000;24:403–15.
- [249] Rosenberg Z, Bless SJ, Brar NS. On the influence of the loss of shear strength on the ballistic performance of brittle solids. *Int J Impact Eng* 1990;9:45–9.
- [250] Rosenberg Z, Bless SJ, Yeshurun Y, Brat NS. On the relation between the penetration resistance of ceramic tiles and their dynamic properties. In: Jono M, Inoue T, editors. Mechanical behaviour of materials 6, vol. 1. Oxford: Pergamon; 1992. p. 507–12.
- [251] Rosenberg Z, Yaziv D, Yeshurun Y, Bless SJ. Shear strength of shock-loaded alumina as determined with longitudinal and transverse manganin gauges. *J Appl Phys* 1987;62:1120–2.
- [252] Rosenberg Z, Brar NS, Bless SJ. Shear strength of titanium diboride under shock loading measured by transverse manganin gauges. In: Schmidt SC, Dick RD, Forbes JW, Tasker DG, editors. Shock compression of condensed matter—1991. Amsterdam: North-Holland; 1992. p. 471–4.
- [253] Brar NS, Rosenberg Z, Bless SJ. Applying Steinberg's model to the Hugoniot Elastic Limit of porous boron carbide specimens. *J Appl Phys* 1991;69:7890–1.
- [254] Mashimo T, Uchino M. Shock compression behavior of boron carbide. In: Schmidt SC, Tao WC, editors. Shock compression of condensed matter 1995. Woodbury, NY: American Institute of Physics; 1996. p. 531–3.
- [255] Moran B, Glenn LA, Kusubov A. Jet penetration in glass. *J Phys IV France* 1991;1(C3):147–56.
- [256] Klopp RW, Shockey DA. The strength behavior of granulated silicon carbide at high strain rates and confining pressure. *J Appl Phys* 1991;70:7318–26.
- [257] Fujii K, Noma T, Masumara O, Mayama T. Dynamic mechanical properties of materials measured by plate impact experiments: Si_3N_4 , SiC and TiB_2 . *JSME Int J A* 2001;44:251–8.
- [258] Synnergren P, Sjö Dahl M. A stereoscopic digital speckle photography system for 3-D displacement field measurements. *Opt Lasers Eng* 1999;31:425–43.
- [259] Synnergren P, Goldrein HT, Proud WG. Application of digital speckle photography to flash X-ray studies of internal deformation fields in impact experiments. *Appl Opt* 1999;38:4030–6.
- [260] Synnergren P, Goldrein HT. Dynamic measurements of internal three-dimensional displacement fields with digital speckle photography and flash X-rays. *Appl Opt* 1999;38:5956–61.
- [261] Goldrein HT, Synnergren P, Proud WG. Three-dimensional displacement measurements ahead of a projectile. In: Furnish MD, Chhabildas LC, Hixson RS, editors. Shock compression of condensed matter—1999. Melville, NY: American Institute of Physics; 2000. p. 1095–8.
- [262] Goldrein HT, Grantham SG, Proud WG, Field JE. The study of internal deformation fields in granular materials using 3D digital speckle X-ray flash photography. In: Furnish MD, Thadhani NN, Horie Y, editors. Shock compression of condensed matter—2001. Melville, NY: American Institute of Physics; 2002. p. 1105–8.
- [263] Grantham SG, Proud WG, Goldrein HT, Field JE. The study of internal deformation fields in granular materials using 3D digital speckle X-ray flash photography. *Proc SPIE* 2000;4101:321–8.
- [264] Grantham SG, Field JE. Speckle correlation methods applied to ballistics and explosives. *Proc SPIE* 2003; 4933:27–32.

- [265] Grantham SG, Proud WG, Field JE. The study of internal deformation fields in materials using digital speckle radiography. *Proc SPIE* 2003;4948:592–7.
- [266] Grantham SG, Goldrein HT, Proud WG, Field JE. Digital speckle radiography: a new ballistic measurement technique. *Imaging Sci J* 2003;51:175–86.
- [267] Ogorodnikov VA, Ivanov AG, Tyunkin ES, Grigorev VA, Khokhlov AA. Dependence of spall strength of metals on the amplitude of a shock-wave load. *Combust Explos Shock Waves* 1992;28:88–92.
- [268] Johnson JN, Gray III GT, Bourne NK. Effect of pulse duration and strain rate on incipient spall fracture in copper. *J Appl Phys* 1999;86:4892–901.
- [269] Nahme H. Spall plane formation near spall threshold for different metals. In: Furnish MD, Chhabildas LC, Hixson RS, editors. *Shock compression of condensed matter—1999*. Melville, NY: American Institute of Physics; 2000. p. 517–20.
- [270] Ogorodnikov VA, Ivanov AG. Time dependence of the fracture energy of metals in spallation. *Combust Explos Shock Waves* 2001;37:119–22.
- [271] Chhabildas LC, Trott WM, Reinhart WD, Cogar JR, Mann GA. Incipient spall studies in tantalum: microstructural effects. In: Furnish MD, Thadhani NN, Horie Y, editors. *Shock compression of condensed matter—2001*. Melville, NY: American Institute of Physics; 2002. p. 483–6.
- [272] Church PD, Proud WG, Andrews TD, Goldthorpe B. The spall strength measurement and modelling of AQ80 iron and copper systems. In: Furnish MD, Thadhani NN, Horie Y, editors. *Shock compression of condensed matter—2001*. Melville, NY: American Institute of Physics; 2002. p. 487–90.
- [273] Ogorodnikov VA. Spalling kinetics over a wide range of shock-wave amplitude and duration. *Combust Explos Shock Waves* 2002;38:484–7.
- [274] Boidin X, Chevrier P, Klepaczko JR. Validation of a fracture model based on mesoscale approach for spalling of hard steel and aluminium alloy. *J Phys IV France* 2003;110:845–50.
- [275] Church P, Cullis I, Bardilas A, Cogar J, Proud WG, Hammond RI. An investigation into spallation of titanium alloy plates using plate impact experiments and simulation. *J Phys IV France* 2003;110:779–84.
- [276] Gray III GT, Bourne NK, Henrie BL, Millett JCF. Influence of shock-wave profile shape (triangular-“Taylor-wave” versus square-topped) on the spallation response of 316L stainless steel. *J Phys IV France* 2003;110:773–8.
- [277] Klepaczko JR, Chevrier P. A meso-model of spalling with thermal coupling for hard metallic materials. *Eng Fract Mech* 2003;70:2543–58.
- [278] Krivtsov AM. Molecular dynamics simulation of impact fracture in polycrystalline materials. *Meccanica* 2003;38:61–70.
- [279] Tonks DL, Zurek AK, Thissell WR. Coalescence rate model for ductile damage in metals. *J Phys IV France* 2003;110:893–8.
- [280] Goldthorpe BD. A path dependent model for ductile fracture. *J Phys IV France* 1997;7(C3):705–10.
- [281] Bourne NK, Forde LC, Field JE. High speed photography and stress gauge studies of the impact and penetration of plates by rods. *Proc SPIE* 1997;2869:626–35.
- [282] Proud WG, Lynch N, Marsh A, Field JE. Instrumented smallscale rod penetration studies: the effect of pitch. In: Crewther IR, editor. *Proceedings of the 19th International Symposium on Ballistics, Interlaken, Switzerland, 2001*. p. 1289–95.
- [283] Cagnoux J, Cauret M, Le Gallic C, Touzé P, Carson WAJ, Cullis IG, Hawkins AJ, Coakley CJ. Penetration of alumina ceramics by tungsten rod penetrators. In: Murphy MJ, Backofen JE, editors. *Proceedings of the 14th International Symposium on Ballistics, vol. 2*. Arlington, VA: American Defence Preparedness Association; 1993. p. 545–54.
- [284] Rosenberg Z, Dekel E, Hohler V, Stilp AJ, Weber K. Hypervelocity penetration of tungsten alloy rods into ceramic tiles: experiments and 2-D simulations. *Int J Impact Eng* 1997;20:675–83.
- [285] Asprey RJ, Edwards MR. Tungsten as a penetrator material. In: Reinecke WG, editor. *Proceedings of the 18th International Symposium on Ballistics*. Lancaster, PA: Technomic Publishing Company, Inc.; 1999. p. 671–8.
- [286] Delagrave R, Nandlall D. Experimental and numerical penetration studies of a scaled kinetic energy penetrator. In: Murphy MJ, Backofen JE, editors. *Proceedings of the 14th International Symposium on Ballistics, vol. 2*. Arlington, VA: American Defence Preparedness Association; 1993. p. 449–58.

- [287] Cullis IG, Lynch NJ. Performance of model scale long rod projectiles against complex targets over the velocity range 1700–220 m/s. *Int J Impact Eng* 1995;17:263–74.
- [288] Peskes GJJM. Scaled long rod experiments on ceramic targets. In: Reinecke WG, editor. *Proceedings of the 18th International Symposium on Ballistics*. Lancaster, PA: Technomic Publishing Company, Inc.; 1999. p. 1089–95.
- [289] Lynch NJ, Brissenden C, Shears PK. Terminal ballistic performance of two novel KE penetrator shapes against oblique semi-infinite RHA. In: Reinecke WG, editor. *Proceedings of the 18th International Symposium on Ballistics*. Lancaster, PA: Technomic Publishing Company Inc.; 1999. p. 1011–8.
- [290] Rae PJ, Goldrein HT, Bourne NK, Proud WG, Forde LC, Liljekvist M. Measurement of dynamic large-strain deformation maps using an automated fine grid technique. *Opt Lasers Eng* 1999;31:113–22.
- [291] Forde LC, Bourne NK, Rosenberg Z, Cornish R, Lynch NJ, Cullis IG, Church PD. Experimental investigation and analysis of penetration in oblique impact. In: *Proceedings of the 16th International Symposium on Ballistics*, vol. 3. Arlington, VA: American Defense Preparedness Association; 1996. p. 641–9.
- [292] Field JE. High speed photography at the Cavendish Laboratory, Cambridge. In: Ray SF, editor. *High speed photography and photonics*. Oxford: Focal Press; 1997. p. 301–14.
- [293] Barker LM. The development of the VISAR and its use in shock compression science. In: Furnish MD, Chhabildas LC, Hixson RS, editors. *Shock compression of condensed matter—1999*. Melville, NY: American Institute of Physics; 2000. p. 11–7.
- [294] Kobayashi AS, editor. *Handbook on experimental mechanics*. Eaglewood Cliffs, NJ: Prentice-Hall; 1987.
- [295] Kobayashi AS, editor. *Handbook on experimental mechanics*, 2nd revised ed. New York: VCH Publishers Inc.; 1993.
- [296] Shukla A, Sadd MH, Mei H. Experimental and computational modeling of wave propagation in antigranulocytes materials. *Exp Mech* 1990;30:377–81.
- [297] Wells AA, Post D. The dynamic stress distribution surrounding a running crack: a photoelastic analysis. *Proc Soc Exp Stress Anal* 1958;16(1):69–96.
- [298] Kalthoff JF. Shadow optical method of caustics. In: Kobayashi AS, editor. *Handbook on experimental mechanics*. Eaglewood Cliffs, NJ: Prentice-Hall; 1987. p. 430–500.
- [299] Manogg P. *Anwendungen der Schattenoptik zur Untersuchung des Zerreißvorgangs von Platten*. PhD thesis, University of Freiburg, 1964.
- [300] Theocaris PS, Gdoutos E. An optical method for determining opening-mode and edge sliding-mode stress-intensity factors. *Trans ASME: J Appl Mech* 1972;39:91–7.
- [301] Zehnder AT, Rosakis AJ. Dynamic fracture initiation and propagation in 4340 steel under impact loading. *Int J Fract* 1990;43:271–85.
- [302] Arakawa K, Drinnon RH, Kosai M, Kobayashi AS. Dynamic fracture analysis by moiré interferometry. *Exp Mech* 1991;31:306–9.
- [303] Deason VA, Epstein JS, Abdallah M. Dynamic diffraction moiré: theory and applications. *Opt Lasers Eng* 1990;12:173–87.
- [304] Whitworth MB, Huntley JM. Dynamic stress analysis by high-resolution reflection moiré photography. *Opt Eng* 1994;33:924–31.
- [305] Huntley JM. Speckle photography fringe analysis: assessment of current algorithms. *Appl Opt* 1989;28:4316–22.
- [306] Huntley JM, Field JE. High speed laser speckle photography. 2: Rotating mirror camera control system and applications. *Opt Eng* 1994;33:1700–7.
- [307] Sutton MA, Wolters WJ, Peters WH, Ranson WF, McNeill SR. Determination of displacements using an improved digital correlation method. *Image Vision Comput* 1983;1:133–9.
- [308] Chu TC, Ranson WF, Sutton MA, Peters WH. Applications of digital-image-correlation techniques to experimental mechanics. *Exp Mech* 1985;25:232–44.
- [309] Sjö Dahl M. Electronic speckle photography: increased accuracy by nonintegral pixel shifting. *Appl Opt* 1994; 33:6667–73.
- [310] Huntley JM, Benckert LR. Measurement of dynamic crack tip displacement field by speckle photography and interferometry. *Opt Lasers Eng* 1993;19:299–312.
- [311] Fallström K-E, Gustavsson H, Molin N-E, Wåhlin A. Transient bending waves in plates studied by hologram interferometry. *Exp Mech* 1989;29:378–87.

- [312] Tippur HV, Krishnaswamy S, Rosakis AJ. A coherent gradient sensor for crack tip deformation measurements: analysis and experimental results. *Int J Fract* 1991;48:193–204.
- [313] Goldrein HT, Palmer SJP, Huntley JM. Automated fine grid technique for measurement of large-strain deformation maps. *Opt Lasers Eng* 1995;23:305–18.
- [314] Burch JM, Forno C. High sensitivity moiré grid technique for studying deformation in large objects. *Opt Eng* 1975;14:178–85.
- [315] Huntley JM, Whitworth MB, Field JE, Benckert LR, Sjödaahl M, Thesken JC, Henriksson A. High resolution moiré photography: application to impact and dynamic fracture of polymers and composites. In: Williams JG, Pavan A, editors. *Impact and dynamic fracture of polymers and composites*. London: Mechanical Engineering Publications Ltd.; 1995. p. 33–44.
- [316] Huntley JM, Palmer SJP, Field JE. Automatic speckle photographic fringe analysis: application to crack propagation and strength measurement. *Proc SPIE* 1987;814:153–60.
- [317] Asay BW, Laabs GW, Hesnon BF, Funk DJ. Speckle photography during dynamic impact of an energetic material using laser-induced fluorescence. *J Appl Phys* 1997;82:1093–9.
- [318] Grantham SG, Field JE. Advances in digital speckle radiography. *Proc SPIE* 2002;4777:159–67.
- [319] Zehnder AT, Rosakis AJ. On the temperature distribution at the vicinity of dynamically propagating cracks in 4340 steel. *J Mech Phys Solids* 1991;39:385–415.
- [320] Mason JJ, Rosakis AJ, Ravichandran G. On the strain and strain rate dependence of the fraction of plastic work converted to heat: an experimental study using high speed infrared detectors and the Kolsky bar. *Mech Mater* 1994;17:135–46.
- [321] Hodowany J, Ravichandran G, Rosakis AJ, Rosakis P. Partition of plastic work into heat and stored energy in metals. *Exp Mech* 2000;40:113–23.
- [322] Walley SM, Proud WG, Rae PJ, Field JE. Comparison of two methods of measuring the rapid temperature rises in split Hopkinson bar specimens. *Rev Sci Instrum* 2000;71:1766–71.
- [323] Guduru PR, Ravichandran G, Rosakis AJ. Observations of transient high temperature vortical microstructures in solids during adiabatic shear banding. *Phys Rev E* 2001;64 (Paper 036128).
- [324] Guduru PR, Rosakis AJ, Ravichandran G. Dynamic shear bands: an investigation using high speed optical and infrared diagnostics. *Mech Mater* 2001;33:371–402.
- [325] Guduru PR, Zehnder AT, Rosakis AJ, Ravichandran G. Dynamic full field measurements of crack tip temperatures. *Eng Fract Mech* 2001;68:1535–56.